Response to reviews, and marked-up manuscript, for "Improvements in one-dimensional grounding-line parameterizations in an ice-sheet model with lateral variations (PSUICE3D v2.1)", by D. Pollard and R.M. DeConto.

We thank the reviewers for their careful and helpful reviews. We agree with all their comments and have acted on all their specific suggestions for changes. Each comment and our response is described below, with the reviewers' text in blue, and our response in black with new manuscript text indented. After that, other changes in the manuscript are described, including our response to the other comment received. Line numbers refer to the revised manuscript with no track changes shown. Finally, a copy of the revised manuscript is included (starting on pg. 10), showing all track changes since the original manuscript submission.

The largest changes are in response to referee 1's suggestion to also compare results for the MISMIP3d intercomparison. This is an excellent suggestion, providing an additional valuable test of the new model modifications. In performing these tests, this led us to a new modification in the grounding-line orientation treatment, as described in the revised Methods section, a new section showing MISMIP3d results, and a new Appendix comparing MISMIP+ and MISMIP3d results for alternate model versions. This is outlined in more detail below.

Referee 1 (F. Pattyn):

The paper presents improvements on a heuristic for grounding-line flux calculations in large-scale ice sheet models. The model initially participated in ice sheet intercomparisons focusing on ideal cases of grounding line behaviour and these published results are now used to improve the algorithm dealing with grounding line motion. The paper definitely valorises the benefit of model intercomparisons that often point to discrepancies or even model errors in some cases. The paper is well written, easy to understand and to follow. However, the paper is technical and therefore of interest for modellers dealing with such type of parameterisations. I would suggest to enlarge the scope a bit in the introduction and explain in some more detail the reasons why such algorithms are necessary, what their advantages and disadvantages are. It would also make a wider readership interested in the problems currently encountered in marine ice sheet modelling.

Lines 19-34: A new opening paragraph is added, providing background and motivation for the use of grounding-line parameterizations in ice-sheet models:

> Accurate modeling of long-term Antarctic Ice Sheet variations requires simulation of ice dynamics in the zone between grounded ice and floating ice shelves, and grounding-line retreat and advance over century and millennial year time scales. Realistic simulation of grounding-line migration is challenging, requiring either higher-order or full-Stokes dynamics (e.g., Seddick et al., 2012), or at least a hybrid combination of horizontally stretching flow (Shallow Shelf Approximation, predominant in shelves and streams) and vertically shearing flow (Shallow Ice Approximation, predominant in inland flow) (e.g., Bueler and Brown, 2009). In any case, sensitivity tests have found that without additional measures, the grounding zone needs to be resolved at fine horizontal resolution on the order of ~100 m to avoid large numerical errors in grounding-line movement (Schoof, 2007; Goldberg et al., 2009; Gladstone et al., 2010, 2012; Pattyn et al, 2012; Cornford et al., 2016). Even with adaptive mesh refinement (Cornford et al., 2013, 2015), long-term $O(10^4$ to 10^6 year) continental-scale simulations are currently computationally infeasible with this approach. Alternately, the ice flux across grounding lines can

be parameterized using an analytic boundary-layer treatment (Schoof, 2007), and embedded in an ice-sheet model (Pollard et al., 2012), making long-term large-scale simulations feasible. This approach performs reasonably well in some idealized model intercomparisons (Docquier et al., 2011; Pattyn et al., 2012; c.f., Gudmundsson, 2013), but less well in others with smaller-scale transient experiments (Pattyn et al., 2013; Pattyn and Durant, 2013; Drouet et al., 2013; Cornford et al., 2020). In this paper we describe new modifications to the parameterized grounding-line flux approach, and show that they significantly improve model performance in some intercomparisons.

I would also suggest to provide a sketch of the proposed simple algorithm for grounding-line direction calculation. Reading through it (page 3 and 4), I took pencil and paper and made a quick drawing. It helped a lot in my understanding.

Line 75: A third panel is added in Fig. 1c providing this sketch. We think it is what the reviewer has in mind, and agree it helps in explaining the algorithm.

I have one major remark/question: both improvements (the grounding line orientation and the weighting scheme on grid velocities) improve the model performance so that it fits within the overall group of models. To what extent is this a clever way of fitting your model to the other models? A way to shed a light on this is to perform the MISMIP3d experiment and compare the result with the same adjustments to the other participating models. As shown in Pattyn and Durand (2013) the heuristic model shows large advance and retreat of the grounding line compared to conventional SSA models at high resolution.

This is an excellent suggestion that had not occurred to us before, and provides an additional valuable test of the new model modifications. In performing these tests, they led us to a new modification in the grounding-line orientation treatment, which produces significantly improved results both for MISMIP+ and MISMIP3d. The new modification involves the calculation of buttressing at the grounding line using the maximum extensional (principal) deviatoric stress over all angles, while still using the grounding-line normal for the direction of the flux. It is described in section 2, lines 138-148:

In Appendix A, results are shown for several variations in calculating N in (4) and θ in (6a). These alternatives stem from the inherent uncertainty in using a 1-D flowline parameterization (Eq. 1) within a 2-D model, and we use the MISMIP+ and MISMIP3d results as an empirical guide. The best overall intercomparison results are obtained not with the above method using the single direction (n_x,n_y) in (4), but using the maximum extensional (principal) stress Nmax, i.e., the maximum of N over all possible directions 0 to 360°, and then

$$\theta = \frac{N_{max}}{\rho_i(1-\rho_i/\rho_w)gh/2} \qquad (6b)$$

For all new-model results in the main paper, N_{max} is used and θ is given by (6b). A rationale for this method is discussed in Appendix A, but we emphasize that the choice is guided mainly because it yields the best overall MISMIP+ and MISMIP3d results among all variations tried (Fig. A1). Note also that N_{max} is used only at the grounding line. In the ice-shelf interior, θ has no effect on the model physics, and where it is shown diagnostically below, the ice velocity at each point provides the orientation in (4).

Note that this new modification is used for all "new" results shown in the main paper, as mentioned in the text (line 72). The main results for MISMIP3d are described in new section 4, on lines 225-241:

> The MISMIP3d intercomparison (Pattyn et al., 2013) offers another useful test of the new model versions. It uses a rectangular fjord-like setting as in MISMIP+, but with a uniformly sloping bed and perturbations in basal sliding coefficient instead of ocean melting. The models are first run to equilibrium, then the basal sliding coefficient is increased (slipperier bed) in a central region for 100 years causing the grounding line to advance, after which the perturbation is removed. Similarly to MISMIP+, our previous model produced larger and more rapid grounding-line advances than most other higher-order and/or higher-resolution models in the intercomparison (Pattyn et al., 2013), and consequently the changes in total volume over flotation and cavity volume differed from most models (Pattyn and Durand, 2013).
>
> Fig. 7a,b shows the main results for the MISMIP3d experiment, for the new model version (solid lines) and the previous standard version close to that used in the original intercomparison. The centerline grounding line excursions in Fig. 7a for the new model version are considerably less than previously (~20 km vs. ~30 km), and much closer to the range of other model categories (red bar on the y-axis, from Pattyn and Durand, 2013). Notably, the equilibrated starting position of the grounding line is now around 560 km, much closer to those of most higher-order models in the intercomparison (~540 km, Pattyn et al., 2013; Pattyn and Durand, 2013).Changes in total volume over flotation and cavity volume in Fig. 7b are also much closer to the ranges of the other model categories (yellow and blue bars on the y-axis; Pattyn and Durand, 2013).
>
> For completeness, spatial maps of changes in surface speed and elevation are shown in Figs. 7c-f, which can be compared with the same quantities for other model categories in Pattyn and Durand (2013) Figs. 2 and 3. There are some differences but the overall features and amplitudes are similar.

Fig. 7 shows our MISMIP3d results, using most of the same types of figures as in Pattyn et al. (2013) and Pattyn and Durand (2013).

In new Appendix A, the main new model version is compared with four alternate modifications in the buttressing calculation. This is new material, and as mentioned in the new text, the modifications stem from the inherent uncertainty in using a 1-D flowine parametrization in a 2-D model. The main point of this Appendix is to show that the "main" modification used in the main text yields the best overall MISMIP+ and MIPSMIP3d results, as shown in Fig. A1. Lines 398-429 (Appendix A) are:

> For all new-model results in the main paper, the buttressing factor θ is given by Eq. (6b), in which the deviatoric normal stress at the grounding line is given by N_{max}, its maximum extensional (principal stress) value over all possible directions 0 to 360^o in Eq. (4). It is a good approximation in the central part of fjord-like channels (Gudmundsson, 2013, Fig. 1); in the shearing margins with stronger buttressing, the resulting θ values still agree reasonably (ibid; his Fig. 2 vs. our Fig. 5). As shown below, this method yields better overall MISMIP+ and MISMIP3d results than all alternatives tried, including simply using the grounding-line normal (n_x,n_y) in Eq. (4) and (6a). We suspect this is because during retreat of an otherwise uniform grounding line in our model, unavoidably there are isolated single grid-cell changes from grounded to floating to ice at each timestep. This produces temporary zig-zags in the grounding line that are not completely muted by the orientation algorithm, and cause spurious single-cell distortions of the flow and overall retreat if θ is given by (6a), which are avoided if θ is given

by (6b). However, we emphasize that the latter method was chosen for the main paper not because of the above rationale, but because it yields the best overall intercomparison results.

Several alternate methods of determining θ are described below, and results are compared with the method using N_{max} and Eq. (6b) as in the main paper. These alternatives stem from the inherent uncertainty in using a 1-D flowline parameterization (Eq. 1) within a 2-D model. Uncertainties in estimating θ in numerical models are also discussed in Gudmundsson (2013). The four alternate methods for calculating N in Eq. (4) and hence θ in Eq. (6) are as follows, labelled A to D:

A. Using the direction (n_x,n_y) normal to the grounding line given by the new orientation algorithm in section 2.
B. Using the direction of ice flow from the preliminary grid-solution (u,v) (also used in Eq. 5).
C. Using maximum N over all directions (Eq. 6b) as in the main paper, but with the strain rates in Eq. (5) calculated for the first ice shelf cell that is entirely surrounded by other ice-shelf cells, looking along a trajectory (n_x,n_y) normal to the grounding line. This avoids "contaminating" the strain rates with velocity points within grounded ice, especially for ice-shelf cells with up to 3 neighboring grounded-ice cells.
D. Using maximum N over all directions (Eq. 6b) as in the main paper, but with the parameterized speed U_g in (1) applied in the direction normal to the grounding line (n_x,n_y), and with the component parallel to the grounding line equal to that of the preliminary grid-solution (cf., Gudmundsson, 2013, Fig. 1).

MISMIP+ and MISMIP3d results for all four methods are shown in Fig. A1. For comparison, thin black lines in each panel show results for the method used in the main paper (Eq. 6b). For MISMIP+, methods A and B yield similar results to the main paper, all within the shaded ranges of the other models. Method C diverges drastically for the Ice1 experiment (Fig. A1c), and method D is nearly outside the range for the Ice2 experiment (Fig. A1h).

For MISMIP3d, methods A and B yield poor results similar to our original MISMIP3d experiments, with considerably larger grounding-line excursions and quite different total changes than the other models. Methods C and D yield almost the same results as the main paper, much closer or within the other model ranges. Hence all four alternate methods A-D yield results that are poorer than that in the main paper, for at least one of the MISMIP+ and MISMIP3d experiments.

The description of the calculation of crevasse depths falls somehow out of the scope of the paper. It is a model improvement but keeps the attention away from the main message and evaluation of the algorithm. furthermore, there is no experimental work presented regarding this modification. I would suggest to leave it out and use it appropriately
in a subsequent manuscript that employs the improvement (typically an appendix).

This minor improvement is now moved to Appendix C, where it is described briefly and a new Fig. C1 shows that it makes negligible difference in the West Antarctic results. Lines 519-526 (Appendix C) are:

For all runs in this paper, an improvement is made in the parameterization of crevasse depths, used both in "normal" calving and also in the cliff-failure physics (Pollard and et al., 2015). Crevasse depths are set to the Nye-depth (at which total horizontal stress is zero for surface crevasses, or is equal to water pressure for basal crevasses; Nye, 1957; Jezek, 1984; Nick et al., 2010). Previously, the divergence $(\partial u/\partial x + \partial v/\partial y)$ was used along with ice viscosity as a simple estimate of the horizontal deviatoric stress (Pollard et al., 2015). Here, this is replaced by the maximum principal deviatoric stress (Turcotte

and Schubert, 1982), calculated from the strain rates and viscosity. This is a small improvement "in principle". It has no effect in the idealized fjord MISMIP+ and MISMIP3d experiments for which calving is disabled, and has negligible effect in the West Antarctic simulations as shown in Fig. C1.

Minor remarks:

Figure 4: please use a different color scheme for the buttressing factor. It is far from obvious to distinguish the colors of the end-members. Why not a scheme similar to the one used in the left panel?

A new color scheme is used in all 2-D maps showing the buttressing factor θ (in Figs. 4, 5, 10, 12). It is red-to-yellow, and we have checked with the reviewer that this is a good scheme. It is different from other color schemes in the paper to distinguish the θ maps from those for other quantities.

Referee 2 (S. Cornford):

This paper described a modification to the 'PSU3D' ice sheet model, which has been used to carry out a wide variety of Antarctic simulations and has been used to produce some of the highest profile results in that field. The model is perhaps the best known of a number that determine an ice flow velocity across the grounding line from a analytic expression derived by Schoof (2007) that applies to 1D flows without buttressing, adapted in some way to higher dimensional flows with buttressing. The signal characteristic of these models is that they perform far better than conventional models (that do not make use of the analytic expression) at low resolution (10 km). Conventional models must be run at far finer resolutions (1 km) to produce plausible results. There are still discrepancies between these groups of models when the conventional models are run at fine resolution, and the modification in this paper addresses the difference that was evident in the MISMIP+ model comparison.

I think this is a good paper that describes its methods well and shows clearly the impact of the modification. I recommend publication, but ask the authors to consider two points (see general comments)

1 General Comments

The modifications described have an impact on the MISMIP+ results (a narrow channel with strongly curved grounding line) but little impact on the (probably more interesting) Antarctic experiments. One interpretation (and the interpretation given here) is that the unmodified model was already computing the relevant quantities well enough . That could be the case. But there is another source of information on this point: the ABUMIP comparison, which is set in Antarctica. This is in review, but the authors of this paper are co-authors of that paper, so are aware of its results . It seems that PSU3D is 'in the envelope' there, as well (at least from the figures I have seen), which seems to be further evidence in support of the author's position. Perhaps it is simply premature to cite a paper that has yet to be published and is not in 'open review', but it seems a shame to miss out on that extra evidence (I see that Frank Pattyn has also reviewed this paper and of course knows the ABUMIP results much better than I, so he may have more to say on that, but I have not looked for the sake of an independent review).

As suggested, we note that the insensitivity of continental-scale Antarctic results to the modifications here is basically consistent with the "within-envelope" behaviour of the model in ABUMIP. This is mentioned in section 5 on West Antarctic results, lines 288-290:

This is consistent with our results in the ABUMIP intercomparison involving continental Antarctic experiments, where the previous model version was used and results lie within the ranges of the other models (Sun et al, 2020).\

and in the concluding section on lines 370-371:

This is borne out by results of pan-Antarctic experiments in the ABUMIP intercomparison (Sun et al., 2020), which lie within the range of the other models.

There is quite a lot of material on brittle failure / cliff collapse (section 5). I don't disagree that ice sheet modellers should be taking these things seriously, but it seems also a bit tangential to the topic of the paper. I don't think it detracts from the paper in any serious sense.

This material is retained without modification (now in renumbered section 6). We think that it is suitable and worthwhile here because its validity is a direct consequence of the improved grounding-line treatment of the paper; i.e., our projections of the future potential for brittle failure in West Antaractica are considerably more robust due to the improved treatment. It demonstrates how idealized intercomparison tests can lead to improved model physics that are central to important real-world applications.

2 Specific Comments

Abstract, L10 "...presumably because dynamics in the wider major Antarctic basins are "adequately represented by the model's previous simpler one-dimensional formulation". see general comments - ABUMIP seems to support the case too.

As noted above, the ABUMIP connection is mentioned in two places in the new text. We do not mention it in the abstract to keep the abstract focused and brief.

L27 "Here we implement a more rigorous," Rigorous (as in mathematical rigour) does not seem like the right word, lacking a formal analysis of error. Complete?

We agree, and have replaced "rigorous" in these places with "realistic" (line 44), "physically complete" (line 46), and "improved" (line 372).

L177 (MISMIP+ experiments). What is the value of A? In MISMIP+, PSU3d used a quite different value from other models to place its initial grounding line. Is that still the case?

Values of the ice rheologic coefficient A in our new MISMIP+ runs are now specified in the caption of Fig. 3. In that figure, three runs are shown for the MISMIP+ Ice1 experiment, and the different A values are discussed in new text on lines 180-186:

Different values of rheologic coefficient A are used as noted in the caption, in order for the equilibrated grounding line at the start of each experiment to have nearly the same x-axis location (~455 km). With the previous model version and original MISMIP+ A value (crosses), the grounding-line variations are close to those in our original MISMIP+ runs, significantly

faster and larger than other higher-order, higher-resolution models as shown in Cornford et al. (2020). With the same model version and a slightly different value of A (thin lines), the results are within the other-model envelopes (background shading), but close to their outer edges; this dependence on A in our model was not noticed before.

The Fig. 3 caption (lines 190-194) is:

Figure 3. Along-fjord centerline position along the x-axis (km) of grounding lines in the MISMIP+ Ice1 experiments (Cornford et al., 2020). **Thick colored lines:** new model version and rheologic coefficient $A = 3 \times 10^{-17}$ Pa^{-3} a^{-1}. **Crosses:** previous model version and $A = 2.5 \times 10^{-17}$ Pa^{-3} a^{-1}. **Thin black lines:** previous model version and $A = 3.5 \times 10^{-17}$ Pa^{-3} a^{-1}. **Green:** control, with zero oceanic melt. **Blue and yellow:** with oceanic melt perturbation. **Red:** with oceanic melt reset to zero after year 100. Shaded regions show the envelopes for the "main subset" of MISMIP+ models, copied from Cornford et al. (2020, their Fig. 7a).

Response to interactive comment (A. Kerkweg, Executive editor):

As requested, the model name and version number are now included in the title: "Improvements in one-dimensional grounding-line parameterizations in an ice-sheet model with lateral variations (PSUICE3D v2.1)". The model code and selected output files are archived and available online, as described in the renamed text section on lines 534-536:

Code and data availability. Selected output files, metadata and model code are available on Penn State's Data Commons archive at http://www.datacommons.psu.edu/commonswizard/MetadataDisplay.aspx?Dataset=6238, and at https://doi.org/10.26208/m3bt-jy63.

Soon after our initial submission to GMDD, we uploaded the original model code and output files corresponding to that submission into that archive. We have now uploaded a new set of code and output corresponding to the revised paper, preserving the original set in its own subdirectory as explained in the archive.

Other changes

The old modification involving "grid-cell weighting of imposed grounding-line velocities" described in section 2.2 of the previous paper is removed, as it was not as well motivated or robust as the others, and would not contribute much to the new paper. (It is replaced by a somewhat analogous modification in the new Appendix B).

The three model versions used for MISMIP+ experiments in the main text of the previous paper (A=old, B=new, C=new plus grid-cell weighting) are replaced in the new paper (old, old with different A, new), which are shown in new Figs. 3 and 6.

The previous paper's Appendix A showing more speculative modifications is replaced by new Appendix B. The three modifications described in new sections B1 to B3 are: (B1) "Strong buttressing", with small θ values prevented from falling to zero, which is related to the previous paper's "grid-weighting" modification removed here as noted above; (B2) "Strain softening", same as old modification A1; (B3) "Overestimate of ice flux…", multiplying U_g by 0.6, same as old modification A2. The new text for section B1 is (lines 451-462):

B1. Strong buttressing

If the buttressing factor θ given by (6) falls to zero or below, this corresponds to compressive horizontal deviatoric stress normal to the grounding line, and compressive (negative) strain in the direction of flow. However, its use in the Schoof formation (1) for grounding-line ice velocity U_g unrealistically predicts very small or zero U_g as θ falls to zero. (Eq. (1a) would be invalid for $\theta < 0$, as noted by Reese et al. (2018); for this equation we reset θ to be within the range [0,1] as mentioned in section 2). This does not occur extensively in our simulations of future Antarctic retreat, because buttressing is generally small as grounding lines rapidly recede into wide interior basins, and is more of a concern in colder climates with expanded grounding lines and shelf ice.

To crudely assess the problem, the value of θ in Eq. (1a) is adjusted for small values so that it does not fall exactly to 0.

If $\theta < 0.3$, then $\theta' = \theta + 0.15\,(\,(0.3-\theta)/0.3\,)^2$ (B1)

(This is applied after θ is reset to the range [0,1] for Eq. (1a)). The adjusted value θ' falls only to 0.15 for strong buttressing, allowing small but non-zero flux. This does not rigorously address the problem, but can provide a guide to its severity by its effect on results.

Like before, these three modifications are compared in new section B4, "Effects on results" (lines 489-500 and 508-511):

B4. Effects on results

The effects of applying each of the modifications described above are shown here. Fig. B1 shows results for the MISMIP+ Ice1 experiment, where the effects are similar in magnitude to those shown in the main paper (Figs. 3). By and large, the grounding-line excursions here are still within in the envelopes of other models in the MISMIP+ intercomparison (Cornford et al, 2020).

For the small-θ modification in Fig. B1a, the differences from the main-paper results are negligible, implying that the shortcomings of the flux parameterization (Eq. 1a) for strong buttressing do not have a large effect on grounding-line migration, at least in fjord-like scenarios. The reason may be that in regions of strong buttressing near the margins, grounding-line fluxes are relatively small, and allowing them to be zero has little effect on the overall evolution (consistent with Gudmundsson, 2013, Fig. 4). For the strain-softening modification in Fig. B1b, there is a serious degradation in results, which now are near the outer edges of the other model envelopes and exhibit spurious fluctuations, indicating this modification is not viable. For the 0.6 U_g modification in Fig. B1c, the results are at least as good as in the main paper, implying that grounding-line migration is not extremely sensitive to uniform changes in the magnitude of the parameterized flux in Eq. (1a).

Fig. B2 shows results for future West Antarctic retreat, for simulations without hydrofracturing or cliff failure. All three modifications described above have very little effects on equivalent sea-level rise, as was also seen in the main paper (Fig.

8); again this is presumably due to the more one-dimensional character of ice retreat in major Antarctic basins, which have wider lateral scales than the MISMIP+ and MISMIP3d channels.

Improvements in one-dimensional grounding-line parameterizations in an ice-sheet model with lateral variations (PSUICE3D v2.1)

David Pollard[1], Robert M. DeConto[2]

[1]Earth and Environmental Systems Institute, Pennsylvania State University, University Park, PA 16802, USA
[2]Department of Geosciences, University of Massachusetts, Amherst, MA 01003, USA

Correspondence to: David Pollard (pollard@essc.psu.edu)

Abstract. The use of a boundary-layer parameterization of buttressing and ice flux across grounding lines in a two-dimensional ice-sheet model is improved by allowing general orientations of the grounding line. This and another modification to the model's grounding-line parameterization are assessed in ~~two~~ three settings: ~~a~~ rectangular fjord-like domains (MISMIP+ and MISMIP3d), and ~~in~~ future simulations of West Antarctic ice retreat under RCP8.5-based climates. The new modifications are found to have significant effects on the fjord-like results, which are now within the envelopes of other models in the MISMIP+ and MISMIP3d intercomparisons. In contrast, the modifications have little effect on West Antarctic retreat, presumably because dynamics in the wider major Antarctic basins are adequately represented by the model's previous simpler one-dimensional formulation. As future grounding lines retreat across very deep bedrock topography in the West Antarctic simulations, buttressing is weak and deviatoric stress measures exceed the ice yield stress, implying that structural failure at these grounding lines would occur. We suggest that these grounding-line quantities should be examined in similar projections by other ice models, to better assess the potential for future structural failure.

1. Introduction

Accurate modeling of long-term Antarctic Ice Sheet variations requires simulation of ice dynamics in the zone between grounded ice and floating ice shelves, and grounding-line retreat and advance over century and millennial year time scales. Realistic simulation of grounding-line migration is challenging, requiring either higher-order or full-Stokes dynamics (e.g., Seddick et al., 2012), or at least a hybrid combination of horizontally stretching flow (Shallow Shelf Approximation, predominant in shelves and streams) and vertically shearing flow (Shallow Ice Approximation, predominant in inland flow) (e.g., Bueler and Brown, 2009). In any case, sensitivity tests have found that without additional measures, the grounding zone needs to be resolved at fine horizontal resolution on the order of ~100 m to avoid large numerical errors in grounding-line movement (Schoof, 2007; Goldberg et al., 2009; Gladstone et al., 2010, 2012; Pattyn et al, 2012; Cornford et al., 2016). Even with adaptive mesh refinement (Cornford et al., 2013, 2015), long-term $O(10^4$ to 10^6 year) continental-scale simulations are currently computationally infeasible with this approach. Alternately, the ice flux across grounding lines can be parameterized using an analytic boundary-layer treatment (Schoof, 2007) and embedded in an ice-sheet model (Pollard et al., 2012), making long-term large-scale simulations feasible. This approach performs reasonably well in some idealized model intercomparisons (Docquier et al., 2011; Pattyn et al., 2012; c.f., Gudmundsson, 2013), but less well in others with smaller-scale transient experiments (Pattyn et al., 2013; Pattyn and Durant, 2013; Drouet et al., 2013; Cornford et al., 2020). In this paper we describe new modifications to the parameterized grounding-line flux approach, and show that they significantly improve model performance in some intercomparisons.

Analytic boundary-layer treatments of buttressing and ice velocities across grounding lines (e.g., Schoof, 2007) are usually 1-D, i.e., formulated with one horizontal dimension along the flowline and no lateral variations. In ice-sheet models with two horizontal dimensions, such formulations can be used to prescribe the approximate flow across grounding lines. In our previous work (Pollard and DeConto, 2012; DeConto and Pollard, 2016), this was done simply by applying the 1-D expressions at individual one-grid-cell-wide segments separating pairs of grounded and floating cells, so that the orientation of each single-cell "grounding-line" segment is parallel to either the *x* or the *y* axis. Although this is consistent with the one-dimensional character of the formulation in Schoof (2007), it ~~neglects~~ does not capture the actual orientation of the wider-scale grounding line~~, and results in non-isotropic buttressing amounts for *x* vs. *y* directions.~~

Here we implement a more realistic~~rigorous, isotropic~~ treatment of grounding-line buttressing and ice flow, by applying the 1-D expressions to normal flow across an estimated ~~more realistic~~ grounding-line orientation that is not constrained to one or the other grid axes. In principle this is more ~~rigorous~~ physically complete than the previous single-cell treatment, and is expected to improve model results. The new grounding-line orientation determines the direction of the ice flux; however, in the calculation of buttressing, overall best results are obtained by using the minimum buttressing over all possible directions, as described below.~~We also implement a modification to improve behavior with strong buttressing, and a minor improvement in crevasse depths, as described below.~~

Three~~wo~~ types of experiments are used to assess the above modifications. First, simulations are performed for a fjord-like glacier confined to a relatively narrow channel, as in the MISMIP+ intercomparison (Cornford et al. 2020). Because of the confining lateral boundaries and a central bedrock depression, grounding lines in these simulations have large two-dimensional curvatures, and provide a good test for the changes implemented here. Second, results are shown for the MISMIP3d intercomparison (Pattyn et al., 2013), also in a fjord-like setting. Third, ~~Second,~~ much larger-scale simulations of future ice retreat in West Antarctica are performed, forced by warming climates corresponding to the extreme RCP8.5 greenhouse gas emissions scenario.

In section 2, the modifications to the buttressing and~~,~~ grounding-line flux ~~and crevasse depth~~ parameterizations are described in detail. Section~~s~~ 3 and 4 present~~s~~ results for the fjord-like MISMIP+ ~~experiments~~and MISMIP3d experiments, respectively. ~~, and S~~section 5~~4~~ presents results~~-~~ of the West Antarctic future simulations~~, comparing results for different combinations of the new model modifications~~. In section 6~~5~~, deviatoric stresses at grounding lines in West Antarctic simulations (without hydrofracturing or cliff-failure physics) are examined, as they retreat across very deep bedrock topography in central West Antarctica in future centuries, to assess the potential for structural failure that could lead to very rapid disintegration of the remaining ice. In ~~an~~ Appendix A, four alternate calculations of buttressing are compared to the omni-directional treatment used in the main paper, showing that the latter yields best overall results for MISMIP+ and MISMIP3d, but they all have very minor effects in the West Antarctic simulations. In Appendix B, ~~two~~three additional ~~additional~~ more speculative~~-~~ modifications to the model's grounding-line flux parameterization are described. Finally, Appendix C describes a minor change used here in the calculation of crevasse depths, based on principal deviatoric stress rather than divergence, which is a small improvement "in principle" but is shown to have insignificant effects in the Antarctic simulations.

2. Methods

~~2.1. Orientation of grounding line~~

As described in Pollard and DeConto (2012), the primary grid in the finite-difference ice-sheet model is the *h*-grid, with ice thicknesses (*h*) defined at the center of each cell. Ice in each *h*-grid cell is either floating in the ocean or is grounded, depending on the ice thickness, bedrock elevation, and sea level. At the grid-cell level, the boundary between floating and grounded-ice regions consists of piecewise-linear segments at the edges between pairs of *h*-grid cells, with each edge parallel to the *x* or *y* axis (Fig. 1a). The model uses an Arakawa-C grid, in which horizontal *u* and *v* velocities are staggered half a grid cell in the *x* and *y* directions respectively, so each segment separating floating or grounded *h*-cells has a *u* or *v* velocity defined at its mid-point, as indicated in Fig. 1a. (The model performs a sub-grid interpolation that refines the grounding-line position between each pair of *h*-grid cells and does not coincide with the cell edge between them, but that does not affect the material presented here).

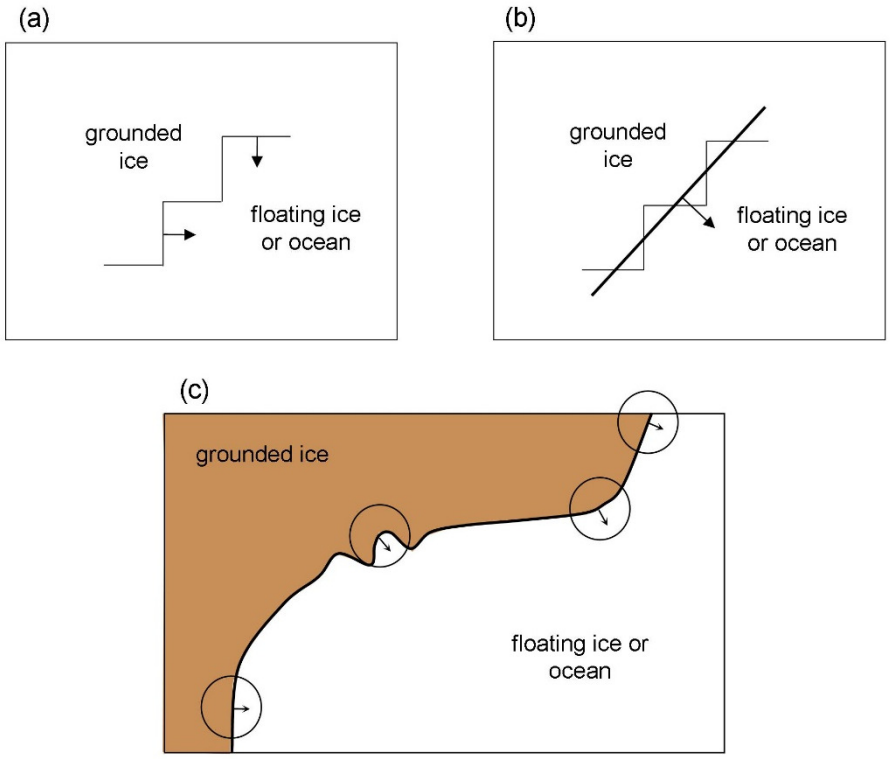

Figure 1. Schematics of grounding-line orientation treatment. Edges of *h*-grid cells are shown by thin lines, with grounded ice on one side (upper left) and floating ice or open ocean on the other (lower right). Ice velocities across grounding lines are shown by arrows. **(a)** Old single-cell piecewise scheme used in ~~earlier~~ previous model versions. **(b)** New scheme with more realistic grounding-line orientation (thicker line). **(c)** New scheme at a larger scale, with the normal at each point determined by the direction towards the center-of-mass of floating ice/ocean points within a given radius.

The model ice dynamics uses a hybrid combination of vertically integrated shallow ice and shallow shelf approximations (SIA, SSA), with the seaward ice flux at grounding lines imposed as a boundary condition according to an analytical expression relating ice flux to ice thickness (Schoof, 2007):

$$q_g = \left(\frac{A(\rho_i g)^{n+1} (1-\rho_i/\rho_w)^n}{4^n C} \right)^{\frac{1}{m+1}} \theta^{\frac{n}{m+1}} \; h^{\frac{m+n+3}{m+1}} \qquad (1a)$$

$$U_g = q_g / h \quad (1b)$$

where q_g is the ice flux and U_g is the ice velocity across the grounding line, and h is ice thickness at the grounding line. ρ_i and ρ_w are the densities of ice and ocean water, respectively, and g is gravitational acceleration. A is the rheological coefficient and n is the exponent for ice deformation. C is the coefficient and m is the exponent for basal sliding (Schoof, 2007), written as C_s and m_s in Pollard and DeConto (2012). The term θ in (1a) represents buttressing by ice shelves, i.e., the amount of back stress caused by pinning points or lateral forces on the ice shelf further downstream. The buttressing factor θ is defined as the ratio of vertically averaged horizontal deviatoric stress normal to the grounding line, relative to its value if the ice shelf was freely floating with no lateral constraints and no back stress. (The latter free-floating value is always extensional, balancing the difference between the column-mean hydrostatic ice pressure at the grounding line with the smaller mean horizontal component of ocean-water pressure on the ice shelf. Pinning points or lateral forces on the ice shelf reduce this value towards zero, i.e., less extensional and more compressive, so $\theta = 1$ for unbuttressed grounding lines and diminishes towards 0 as buttressing increases.)

The analysis for grounding-line flux and buttressing in Schoof (2007) is limited to one-dimensional flowline geometry. In our previous "standard" model (Pollard and DeConto, 2012), Eq. (1) is applied across individual one-grid-cell-wide segments separating pairs of grounded and floating grid cells, so that the orientation of each single-cell "grounding-line" segment is parallel to either the x or the y axis, as sketched in Fig. 1a. In the standard model, the buttressing factors θ_u and θ_v in the x and y directions respectively are:

$$\theta_u = \frac{4\,\eta(\partial u/\partial x)\,h}{\rho_i(1-\rho_i/\rho_w)gh^2/2} \quad (2a)$$

$$\theta_v = \frac{4\,\eta(\partial v/\partial y)\,h}{\rho_i(1-\rho_i/\rho_w)gh^2/2} \quad (2b)$$

where η is the non-linear strain-dependent ice viscosity, and the numerators in (2a,b) are 2x the deviatoric stress (times ice thickness h) in the x or y directions.

Although this previous treatment of θ is consistent with the one-dimensional character of the formulation in Schoof (2007), it does not capture the wider-scale orientation of the real grounding line, which does not actually run along the "staircase" single-cell segments as in Fig. 1a. ~~Furthermore, it results in non-isotropic θ values for the u and v staggered-grid velocities.~~

A~~n alternative~~ new method~~treatment~~ for~~of~~ the direction of U_g and the value of θ is described below, and sketched in Fig. 1b and 1c. ~~The new method~~ It allows for general grounding-line orientations running at an angle to the grid axes, and applies the ice flux given by (1) in a direction normal to this grounding line. First, an estimate of the grounding-line orientation is needed, that represents a spatial smoothing of the boundaries of nearby cells. A simple algorithm is used, as follows.

(i) Consider all grid cells within a given radius R_c of the location in question (x_c, y_c), and take the average of the x and y coordinates of cells with ocean or floating ice (not grounded ice), (x_o, y_o). If this radius extends beyond the domain boundaries, virtual points are used with their grounded or floating property equal to that extended normally from the domain boundary.

(ii) Then the normal to the grounding line (in the direction towards the ocean) is (x_o - x_c, y_o - y_c). The length of this vector is normalized to 1 meter, and is called (n_x,n_y) below.

The resulting grounding-line orientations in some MISMIP+ experiments are shown below, which show that the algorithm works as expected. The choice of radius R_c distinguishes small-scale sinuosities in the grounding line that are averaged out, and larger-scale curvilinear features that should be retained. For the relatively confined fjord MISMIP+ experiments below, R_c is set to 20 km, and for the much larger-scale Antarctic simulations it is set to 50 km. In sensitivity tests (not shown), choices of R_c between 10 to 50 km make very little difference to the results in both types of experiments.

This orientation is used for the direction of the grounding-line velocity (Eq. 7 below). It can also be used in the calculation of N, the net deviatoric stress normal to the grounding line, and hence θ. The equations below follow Gudmundsson (2013, his Eqs. 2, 6 and 12).

$$N = \hat{\boldsymbol{n}}^T . (\boldsymbol{T} . \hat{\boldsymbol{n}}) \tag{3}$$

where $\boldsymbol{T}$ is the deviatoric stress tensor (Gudmundsson, 2013) and $\hat{\boldsymbol{n}}$ is the unit vector (n_x,n_y) normal to the grounding line provided by the algorithm above. Expanding in x,y coordinates, this is:

$$N = \left(2\tau_{xx} + \tau_{yy}\right) {n_x}^2 \; + \; 2\tau_{xy} n_x \, n_y \; + \; \left(2\tau_{yy} + \tau_{xx}\right) {n_y}^2 \tag{4}$$

where τ_{ij} are the 2D components of the stress tensor, obtained from the corresponding strain rates and viscosity η (e.g., Thoma et al., 2014):

$$\tau_{xx} = 2\eta \, \partial u/\partial x, \qquad \tau_{yy} = 2\eta \, \partial v/\partial y, \qquad \tau_{xy} = 2\eta \, (\partial u/\partial y + \partial v/\partial x)/2 \tag{5}$$

These velocities u,v are obtained from a preliminary solution of the SSA dynamical equations performed at each timestep without any Schoof-imposed constraints at the grounding line (Pollard and DeConto, 2012), called the "grid-solution" below. Then the buttressing factor θ is given by

$$\theta = \frac{\sout{N_{max}} N}{\rho_i (1-\rho_i/\rho_w) g h/2} \tag{6a}$$

The denominator is the net normal deviatoric stress that would result for a freely floating and completely unbuttressed ice shelf (or a vertical ice face with no ice shelf at all). ~~θ is used in Eq. (1) to obtain the imposed ice flux q_g and velocity U_g normal to the grounding line.~~

In Appendix A, results are shown for several variations in calculating N in (4) and θ in (6a). These alternatives stem from the inherent uncertainty in using a 1-D flowline parameterization (Eq. 1) within a 2-D model, and we use the MISMIP+ and MISMIP3d results as an empirical guide. The best overall intercomparison results are obtained not with the above method using

the single direction (n_x,n_y) in (4), but using the maximum extensional (principal) stress N_{max}, i.e., the maximum of N over all possible directions 0 to 360°, and then

$$\theta = \frac{N_{max}}{\rho_i(1-\rho_i/\rho_w)gh/2} \quad (6b)$$

For all new-model results in the main paper, N_{max} is used and θ is given by (6b). A rationale for this method is discussed in Appendix A, but we emphasize that the choice is guided mainly because it yields the best overall MISMIP+ and MISMIP3d results among all variations tried (Fig. A1). Note also that N_{max} is used only at the grounding line. In the ice-shelf interior, θ has no effect on the model physics, and where it is shown diagnostically below, the ice velocity at each point provides the orientation in (4).

The value of θ from (6a) or (6b) can be less than 0 or greater than 1 (Gudmundsson, 2013) as shown in the figures below. However, when used in Eq. (1) to obtain the imposed flow across the grounding line U_g, it is restricted to the range [0,1], i.e, reset to max (0, min (1,θ)). Finally, U_g ~~(in the direction (n_x,n_y))~~ is resolved into its x- and y-axis components, using the orientation (n_x,n_y) from the algorithm above:

$$u_g = U_g\, n_x \quad (7a)$$

$$v_g = U_g\, n_y \quad (7b)$$

These velocity components are imposed in the final SSA solution at each time step, at staggered u or v-grid points as appropriate located at the mid points between pairs of grounded and floating h-grid cells. (It is easy to show that this decomposition of U_g onto the u and v-grids results in the physically correct net flux across the actual grounding line, averaged over many u and v-grid points).

As well as entering in the Schoof grounding-line flux Eq. (1a), the buttressing factor θ also affects the effects of crevasses and hydrofracturing in grounding-zone cliff-failure (Pollard et al., 2015). These physics are not enabled for all MISMIP+ runs and most of the Antarctic runs below.

~~**2.2. Grid-cell weighting of imposed grounding-line velocities**~~

~~If the buttressing factor θ falls to zero or below in (6), this corresponds to net zero or compressive horizontal deviatoric stress normal to the grounding line, and zero or compressive (negative) strain in the direction of flow. However, its use in the Schoof formation for grounding line ice velocity (1) predicts zero velocity for $\theta = 0$, and becomes invalid for $\theta < 0$, as noted by Reese et al. (2018). In our application, θ in Eq. (1a) is restricted to be greater or equal to 0, but can still unrealistically cause the Schoof velocity U_g to become very small or zero if θ falls to 0.~~

~~To avoid this problem, here we modify the condition (Box 9 in Pollard and DeConto, 2012) that selects the grid cell location at which the Schoof grounding line velocity components u_g or v_g from (7) are imposed. First, we describe this condition in the~~

standard model. The following is written with all variables and indices for u velocities on the u grid, but it applies equally to v velocities on the v grid.

The condition affects whether u_g is applied at the u grid point separating a pair of floating vs. grounded h grid cells, or at the next downstream u grid point. The choice depends on the difference $u_g - u_{grid}$, where u_{grid} is the "grid solution" velocity from a preliminary solution of the SSA equations without Schoof constrains, as mentioned above. The grounding line is assumed to be retreating if $u_g >> u_{grid}$, and be advancing if $u_g << u_{grid}$. If the former, u_g is imposed at the "actual" grounding line location between the pair of grounded vs. floating h grid points, and if the latter, u_g is imposed at the next downstream (floating) location. This rule is ad hoc, but yields reasonable grounding line migration in idealized tests and real world simulations. It works because in probable advancing situations with relatively small u_g, it is applied at the downstream edge of the first floating h grid cell, generally allowing it to thicken towards grounding; and in probable retreating situations with relatively large u_g, it is applied at the downstream edge of the last grounding h grid cell, generally allowing it to thin towards flotation.

To implement this condition, a weighting factor w (0 to 1) is used:

$$w = \max\left[0,\ \min\left[1,\ \left(u_g - u_{grid}\right)/U_{norm}\right]\right] \quad (8)$$

where the normalizing velocity $U_{norm} = (10^5\ \mathrm{m^2\ yr^{-1}}) / h_g$, and h_g is the ice thickness at the grounding line. In early model versions described in Pollard and DeConto (2012, Box 9), this was imposed as a binary choice with w either 0 or 1, i.e., as if U_{norm} in (8) was very small. In more recent model versions the gradual weighting in (8) has been used, which was found to yield smoother behavior in some tests.

The SSA equations for (u,v) over the whole domain are solved with the following impositions at the two grounding zone points mentioned above, denoted here by u grid indexes *iau* between a grounded vs. floating h grid pair, and *ibu* at the next u grid point downstream (all on the x-axis, with the y-axis index j not shown). In the standard model used to date:

At *iau*: $w.u_g$, $(1-w)$.[*SSA equation terms at iau*] (9a)

At *ibu*: $(1-w).u_g$, w.[*SSA equation terms at ibu*] (9b)

In the SSA sparse matrix and right hand side of the equation for u at grid point (*iau*, *j*), the first quantity of the pair in Eq. (9a) is used to weight u towards u_g with weight w, and the second quantity indicates that all other quantities (which would yield the non-Schoof "grid solution") are multiplied by $1-w$. The same is done for u at point (*ibu*, *j*), using Eq. (9b) with w and $1-w$ switched.

Here, we introduce a slight modification to the weighting, aimed at avoiding the problem of u_g becoming zero as θ falls to zero in Eq. (1):

At *iau*: $w.u_g$, $(1-w)$.[*SSA equation terms at iau*] (10a)

At *ibu*: $(1-w).u_{grid}(iau)$, w.[*SSA equation terms at ibu*] (10b)

~~The only difference from the standard model is the use in (10b) of $u_{grid}(iau)$ at point *ibu* instead of u_g. This term is weighted by 1-w, so is significant in probable advancing situations with small u_g (w close to 0); the use of $u_{grid}(iau)$ at *ibu* still allows the first floating h grid cell to thicken sufficiently towards grounding. In the old model, as u_g falls to zero and w falls to zero, the imposed velocity at *ibu* in (9b) also falls to zero. In the new model, the imposed velocity in (10b) does not tend to zero, which is more reasonable. Instead, the divergence $\partial u/\partial x$ between *iau* and *ibu* tends to zero, as it should for strong buttressing causing θ to fall towards zero.~~

3. Results: MISMIP+ experiments

As a first test of the modifications above, we use the MISMIP+ experiments (Cornford et al., 2020). These simulate glacier flow in a rectangular fjord-like channel, and involve significant two-dimensional curvatures of grounding lines. The channel is 80 km wide, with bedrock generally sloping downstream and an ice shelf flowing into the ocean. There is a bedrock depression at mid-fjord around $x \approx 400$ km, and a ridge at $x \approx 505$ km, as shown in Fig. 2. All prescribed fields and model solutions are laterally symmetric about the centerline of the channel. Starting from a close-to-equilibrated control state with the centerline grounding line just downstream of the bedrock depression, prescribed perturbations to sub-ice oceanic melt rates (which are zero in the control) are applied for 100 years, and either maintained or re-set to zero for the next 100 years. In the MISMIP+ Ice1 experiment, the applied oceanic melt rate is a smooth function of ice-shelf draft and ocean depth, and in the Ice2 experiment, it is a large uniform value in the downstream section of the fjord (Cornford et al., 2020). The resulting variations of the grounding line are examined, mainly its position along the centerline of the channel. All MISMIP+ runs here use a model resolution of 1 km; results at 2 km~~, or 2 km where noted; results~~ are very similar ~~at these resolutions~~. At 5 km and coarser resolutions, in some runs ~~the~~ the curvilinear features in the fjord are not adequately resolved (with only 8 grid points or less in each channel half-width), and results are physically unreasonable.

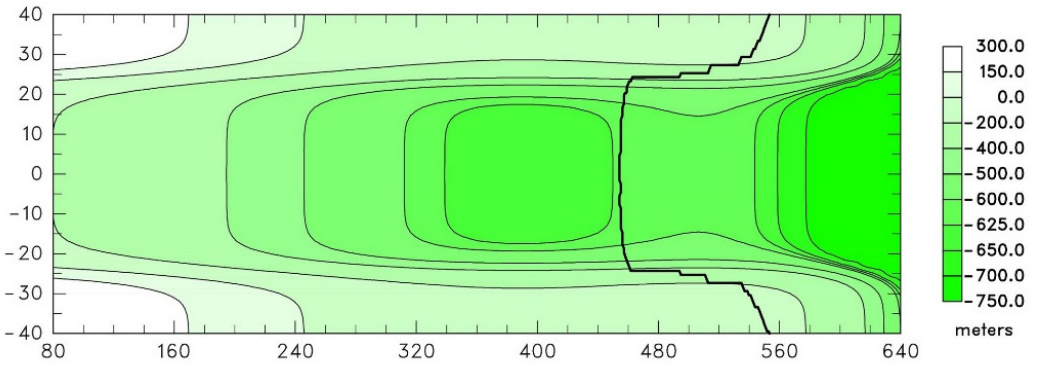

Figure 2. Bedrock topography used in the MISMIP+ experiments (Cornford et al, 2020). Also shown is the "control" grounding line after spin-up at year 0 (thick black line). Axes scales are in km. The first 80 km of the channel is not shown. Note the nearly 3x stretching of the channel width relative to the length.

~~With our standard model, i.e., without any of the modifications above, the grounding line variations were significantly faster and larger than other higher order, higher resolution models in the intercomparison (Cornford et al, 2020). Here, we perform various sensitivity experiments with one or more of the modifications above:~~

~~A. the previous model with single-cell "staircase" grounding lines (Eq. 2).~~

~~B. the 2-D grounding-line orientation in section 2.1 (Eqs. 3 to 7).~~

~~C. the 2-D orientation, and the improved grid-cell weighting in section 2.2 (Eq. 10).~~

Fig. 3 shows results for the MISMIP+ Ice1 experiment, comparing the new model version with our previous standard model; the latter is very close to that used in the original intercomparison (Cornford et al., 2020) ~~with the three model versions A to C~~. Different values of rheologic coefficient A are used as noted in the caption, in order for the equilibrated grounding line at the start of each experiment to have nearly the same x-axis location (~455 km). With the previous model version and original MISMIP+ A value (~~crosses~~thin black lines), the grounding-line variations ~~along the centerline~~ are close to those in our original MISMIP+ runs, ~~those in our earlier experiments shown in Cornford et al. (2020~~ significantly faster and larger than other higher-order, higher-resolution models as shown in Cornford et al. (2020). With the same model version and a reduced value of A (crosses), the results are within the other-model envelopes (background shading), but close to their outer edges; this dependence on A in our model was not noticed before. With the new model version and an intermediate value of A (thick lines), ~~each new modification (B, thin lines; C, thick lines),~~ the grounding-line variations are considerably less rapid and have smaller amplitudes, ~~. Both modifications cause a similarly sized change. In both new experiments, the results in Fig. 3~~ and lie well within the envelopes of the other higher-order, higher-resolution models in the intercomparison ~~MISMIP+ intercomparison for Ice1 (shown as background shading in Fig. 3)~~. This suggests that the modifications above are real physical improvements to our model.

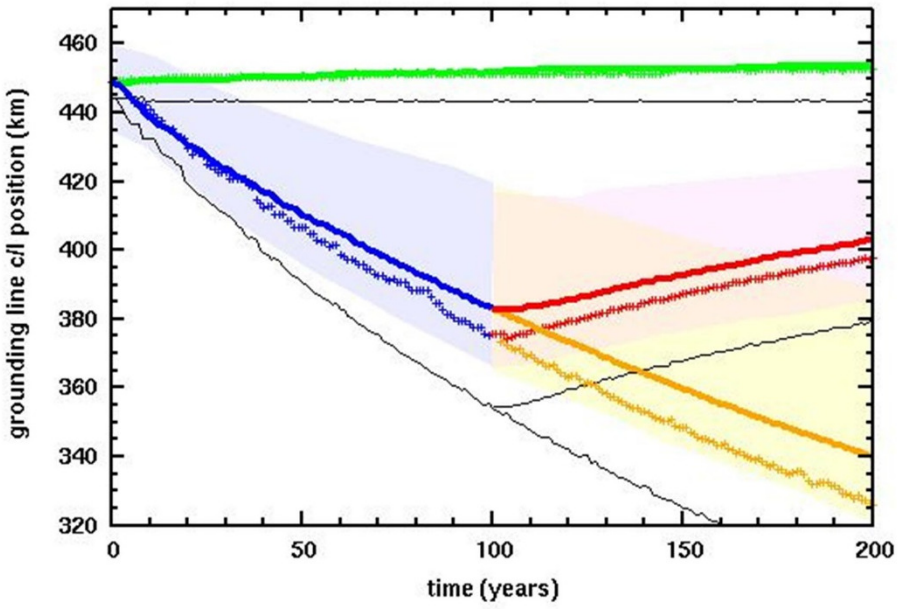

Figure 3. Along-fjord centerline position along the x-axis (km) of grounding lines in the MISMIP+ Ice1 experiments (Cornford et al., 2020). **Thick colored lines:** ~~with~~ new model version and rheologic coefficient A = 3 x 10^{-17} Pa^{-3} a^{-1} ~~2-D orientation and new grid-cell weighting of imposed grounding-line velocities (section 2.2, version C)~~. ~~**Thin lines**~~**Crosses:** ~~with new~~previous model version and A = 2.5 x 10^{-17} Pa^{-3} a^{-1} ~~2-D grounding-line orientation (section 2.1, version B).~~ ~~**Crosses**~~**Thin black lines:** ~~with~~ previous ~~"standard"~~ model version and A = 3.5 x 10^{-17} Pa^{-3} a^{-1} ~~(no modifications, version A)~~. ~~**Thin lines:** with new 2-D grounding-line orientation (section 2.1, version B).~~ **Green:** control, with zero oceanic melt. **Blue and yellow:** with oceanic melt perturbation. **Red:** with oceanic melt reset to zero after year 100. Shaded regions show the envelopes for the "main subset" of MISMIP+ models, copied from Cornford et al. (2020, their Fig. 7a).

Spatial maps of ice extents, grounding lines, and buttressing factors are shown in Fig. 4~~, just~~ for the new model version~~n, C with both new modifications,~~ at the beginning and end of each 100-year segment. Away from the margins, the grounding-line configurations are quite similar to those for other~~most~~ models shown in Cornford et al. (2020); however, near the margins our grounding lines extend further downstream (to ~550 km) than most other models (~490 to 520 km). The buttressing factors in the right-hand column, not adjacent to the grounding line, are purely diagnostic and have no effect on the model physics. As noted above, t~~T~~hey are computed from~~with~~ Eqs. (4) to ~~s. (3) to~~ (6a)~~, but~~ using~~using~~ the direction of ice flow as the normal vector in Eq. (4) ~~instead of the grounding-line orientation algorithm~~ (cf. Fürst et al., 2016).

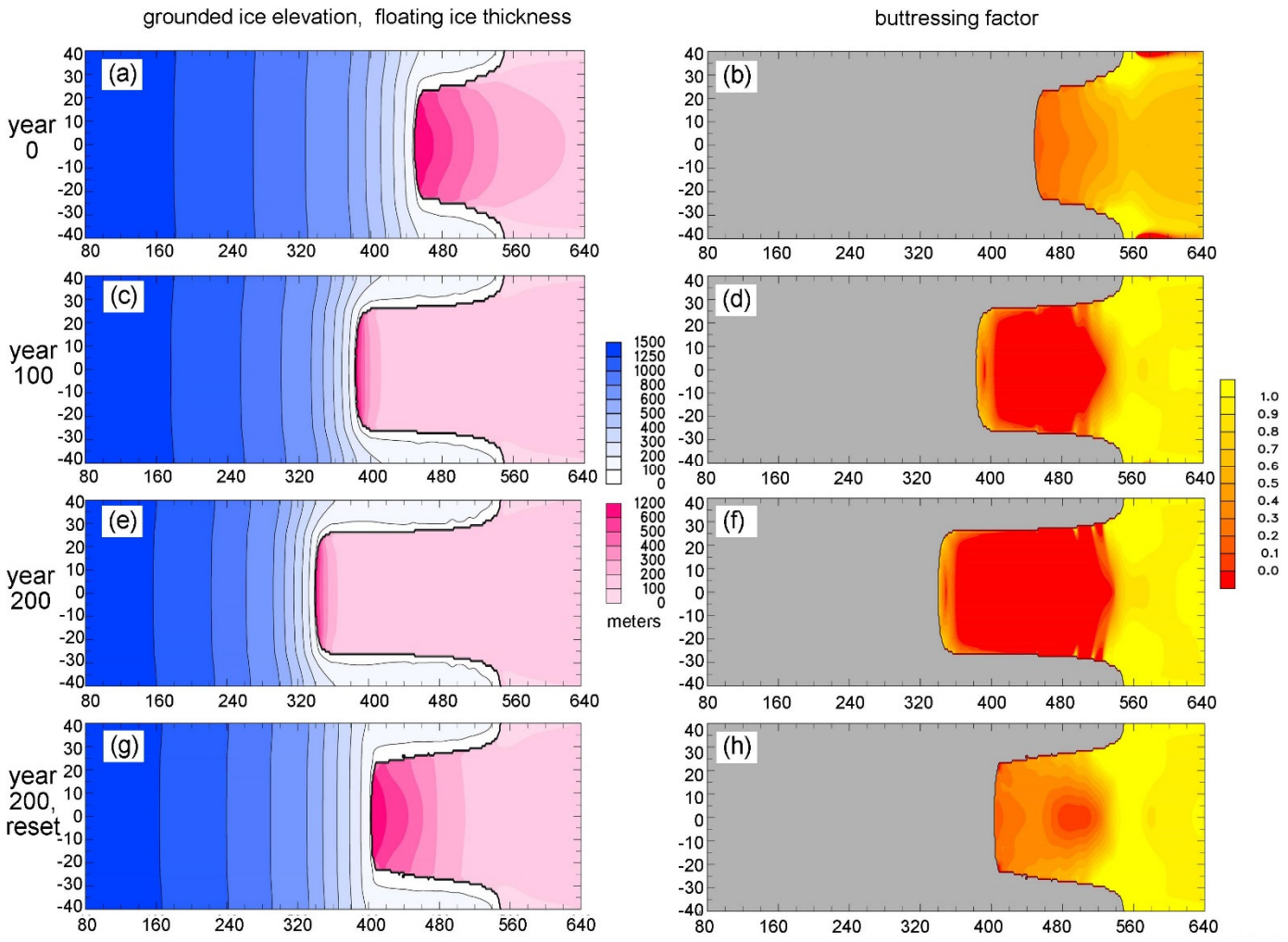

Figure 4. Spatial maps in the MISMIP+ Ice1 experiments, for the new model version (as in Fig. 3 with A = 3 x 10^{-17} Pa^{-3} a^{-1}~~ C with both new modifications.~~). Flow is left to right. The grounding line is shown by a thick black line. The axes scales (km), truncation of first 80 km, and stretched width are as in Fig. 2. ~~Model resolution is 2 km for better visibility of quantities in Fig. 5.~~ **1st row (a-b):** at year 0 (control). **2nd row (c-d):** at year 100 with oceanic melt perturbation. **3rd row (e-f):** at year 200 with oceanic melt perturbation. **4th row (g-h):** at year 200 with oceanic melt reset to zero after year 100. **1st column (a,c,e,g):** Grounded ice surface elevations (m, blue scale), and floating ice thicknesses (m, pink scale). **2nd column (b,d,f,h):** Buttressing factor θ (diagnostic except at grounding line).

Fig. 5 shows buttressing factors and grounding-line orientations, as in Fig. 4 but just at the grounding lines. The ~~left~~right-hand panels (buttressing factors) compare favorably with similar plots in Gudmundsson (2013, his Fig. 2). The ~~right~~left-hand panels

(grounding-line orientations) shows that the simple algorithm described in section 2.~~1~~ works well and yields appropriate angles for these geometries.

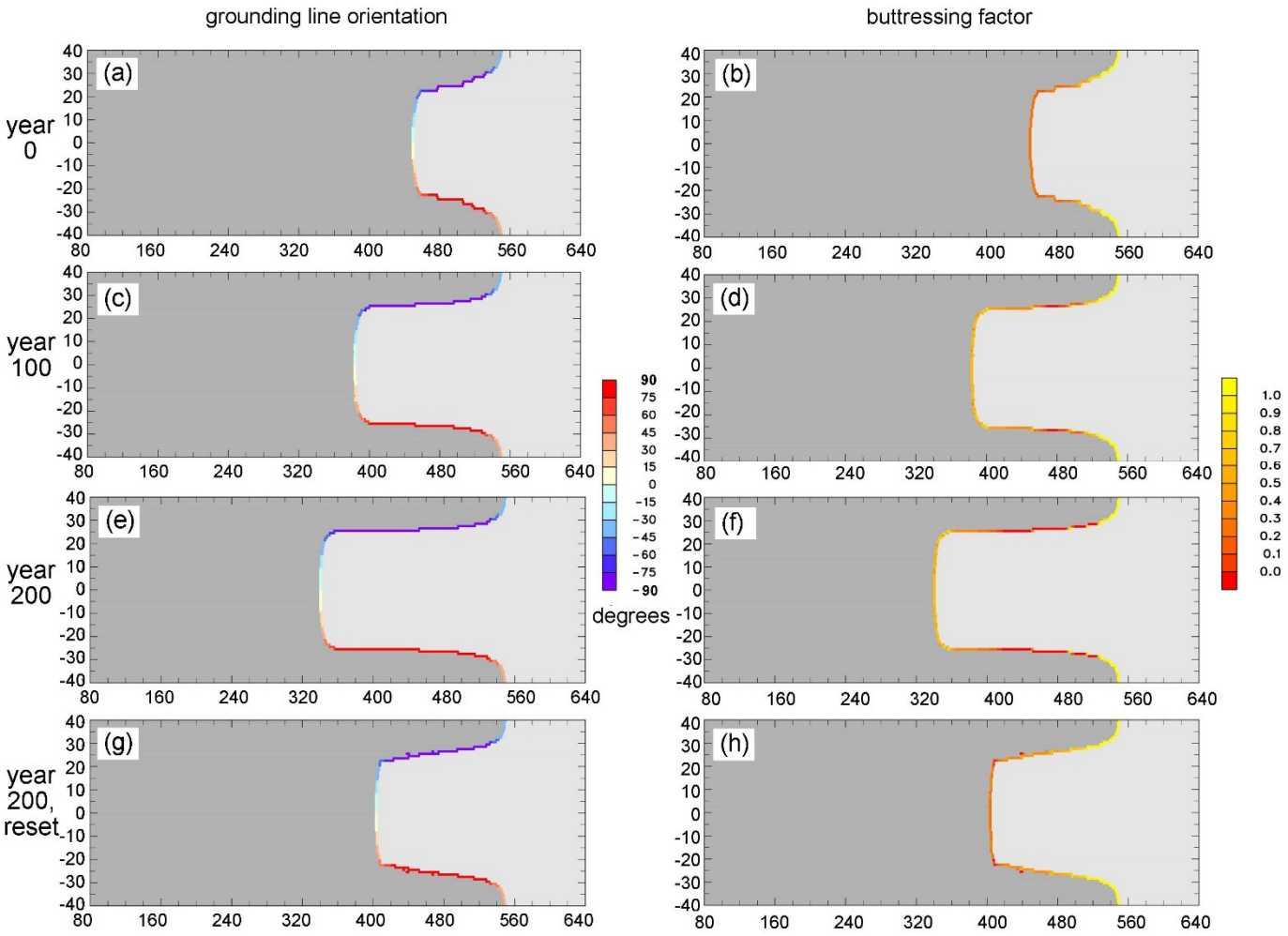

Figure 5. As Fig. 4 for quantities at grounding lines. ~~**1st column (a,e,e,g):** Buttressing factor θ. **2nd column**~~**1st column** (**a,c,e,g~~b,d,f,h~~**):** Orientation of grounding line (degrees counterclockwise of normal vector (n_x,n_y) from the along-fjord x axis, given by algorithm in section 2.~~1~~). ~~**1st** **2nd column (b,d,f,h~~a,c,e,g~~):** Buttressing factor θ.

Centerline grounding-line variations for the Ice2 MISMIP+ experiment, with a spatially abrupt oceanic melt pattern, are shown in Fig. 6 for the same ~~three~~ model versions as in Fig. 3~~6~~. The modifications have ~~much the same~~similar effects as in Fig. 3 for the Ice1 experiment, reducing the rapidity and amplitude of the grounding-line variations compared to the ~~our~~ previous model version with the original rheologic coefficient A (thin black lines). However, results with ~~As for Ice1,~~the previous model version and reduced A (crosses) and the new model version with intermediate A (thick colored lines) are nearly the same here, and both ~~our new Ice2 results now~~ lie well within the envelopes of other MISMIP+ models (Cornford et al., 2020).

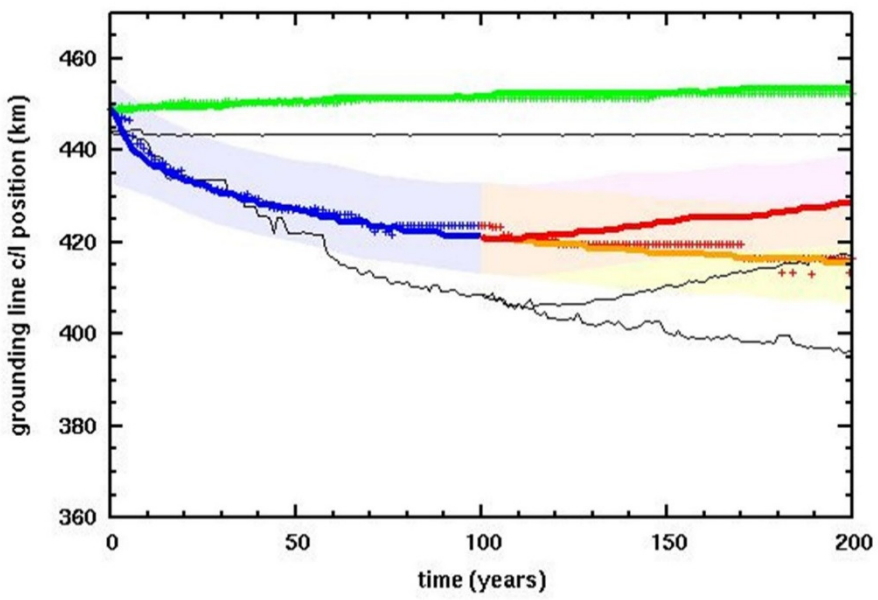

Figure 6. As Fig. 3 except for the MISMIP+ Ice2 experiments. ~~,~~S ~~with s~~hading for the "main subset" of MISMIP+ models is~~,~~ copied from Cornford et al. (2020, their Fig. ~~12b~~13b).

4. Results: ~~West Antarctic simulations~~ MISMIP3d experiments

The MISMIP3d intercomparison (Pattyn et al., 2013) offers another useful test of the new model versions. It uses a rectangular fjord-like setting as in MISMIP+, but with a uniformly sloping bed and perturbations in basal sliding coefficient instead of ocean melting. The models are first run to equilibrium, then the basal sliding coefficient is increased (slipperier bed) in a central region for 100 years causing the grounding line to advance, after which the perturbation is removed. Similarly to MISMIP+, our previous model produced larger and more rapid grounding-line advances than most other higher-order and/or higher-resolution models in the intercomparison (Pattyn et al., 2013), and consequently the changes in total volume over flotation and cavity volume differed from most models (Pattyn and Durand, 2013).

Fig. 7a,b shows the main results for the MISMIP3d experiment, for the new model version (solid lines) and the previous standard version close to that used in the original intercomparison. The centerline grounding line excursions in Fig. 7a for the new model version are considerably less than previously (~20 km vs. ~30 km), and much closer to the range of other model categories (red bar on the y-axis, from Pattyn and Durand, 2013). Notably, the equilibrated starting position of the grounding line is now around 560 km, much closer to those of most higher-order models in the intercomparison (~540 km, Pattyn et al., 2013; Pattyn and Durand, 2013). Changes in total volume over flotation and cavity volume in Fig. 7b are also much closer to the ranges of the other model categories (yellow and blue bars on the y-axis; Pattyn and Durand, 2013).

For completeness, spatial maps of changes in surface speed and elevation are shown in Figs. 7c-f, which can be compared with the same quantities for other model categories in Pattyn and Durand (2013) Figs. 2 and 3. There are some differences but the overall features and amplitudes are similar.

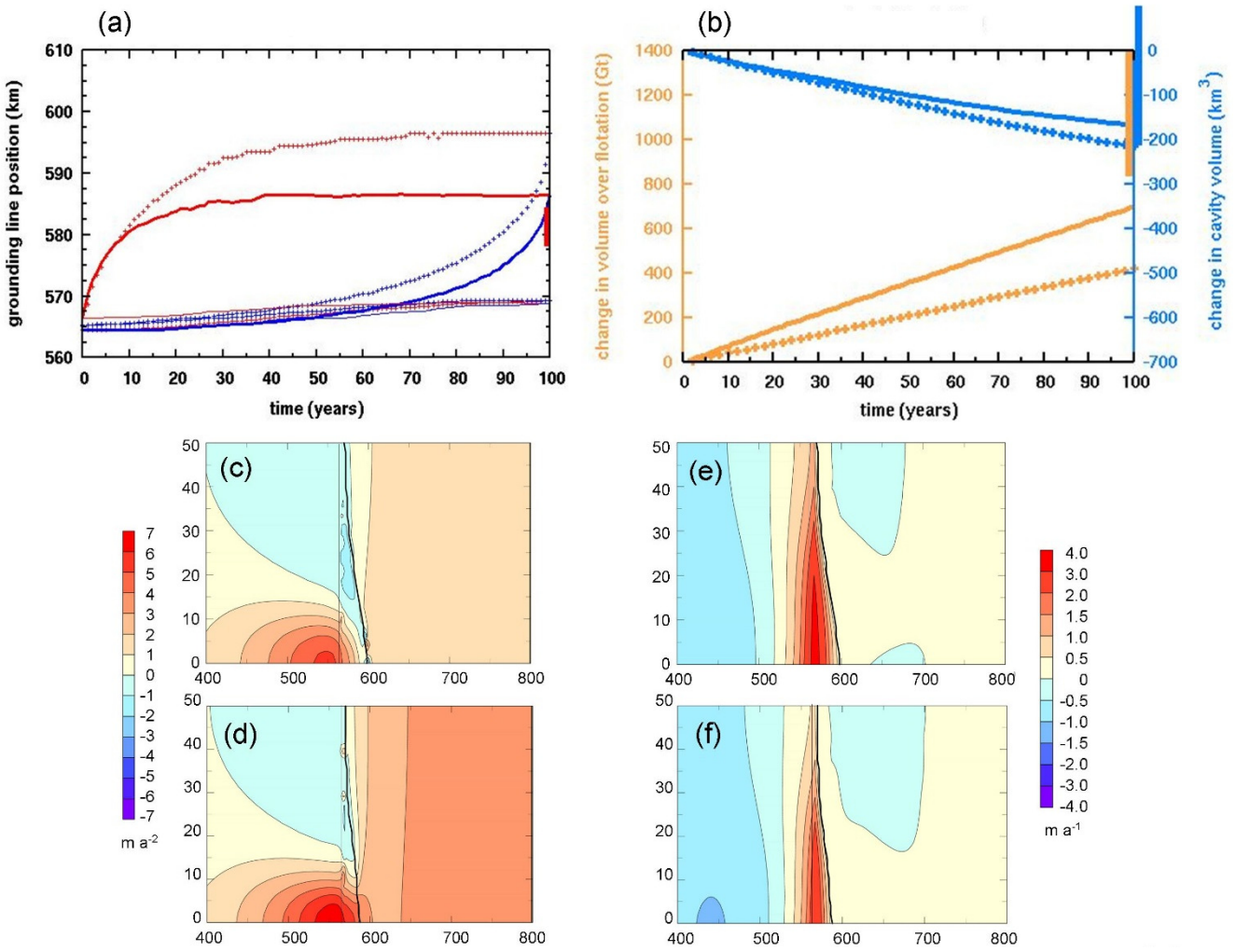

Figure 7. (a) Along-fjord position along the domain x-axis (km) of grounding lines in the MISMIP3d experiment (Pattyn et al., 2013). **Solid lines:** new model version. **Crosses:** previous model version. **Red:** advancing grounding lines for 100 years after the perturbation. **Blue:** retreating grounding lines after the perturbation is removed (reverse time axis). Thick upper lines show centerline positions, and thin lower lines show positions at the domain edge. The vertical red bar on the right-hand y-axis shows the range of amplitude of centerline excursions at 100 years for other model categories in the intercomparison (from Pattyn and Durand, 2013, Fig. 1). **(b) Yellow:** Changes in total ice volume over flotation (multiplied by ice density, Gt of ice), for a half-domain from the centerline to one *y*-axis edge (as in Pattyn and Durand, 2013). **Blue:** Changes in total cavity volume under floating ice (km^3), for the same half-domain (ibid). Solid lines vs. crosses denote new vs. previous model versions as in (a). The vertical yellow bar on the right-hand y-axis shows the volume-over-flotation range at year 100 for the other model categories in the intercomparison, and the vertical blue bar shows the same range for cavity volume (from Pattyn and Durand, 2013, Fig. 4). **(c,d):** Mean rate of change in ice surface speed from year 0 to year 100 (m a^{-2}) as in Pattyn and Durand (2013, Fig. 2). **(e,f)**: Mean rate of change in ice surface elevation from year 0 to year 100 (m a^{-1}) as in Pattyn and Durand (2013, Fig. 3). **(c,e)** are for the previous model version, and **(d,f)** are for the new model version. In (c-f), thin and thick black lines show the position of the grounding line at years 0 and 100, respectively.

5. Results: West Antarctic simulations

To test the modifications in real-world scenarios at larger scales than the idealized fjord experiments above, we simulate retreat of the West Antarctic ice sheet due to future climate warming. The climate forcing follows that in DeConto and Pollard (2016)

for the extreme RCP8.5 greenhouse gas emissions scenario, with atmospheric temperatures and precipitation from regional climate model simulations, and oceanic temperatures from a transient future simulation with the NCAR CCSM4 global climate model (Shields et al., 2017). The ice sheet is initialized to modern observed (Fretwell et al., 2013), and run from 1950 CE for 500 years. A nested domain is used spanning West Antarctica with a polar stereographic grid of 10 km resolution, and with lateral boundary conditions supplied by an earlier continental-scale run.

The mechanisms of hydrofracturing and cliff-failure (Pollard et al., 2015; DeConto and Pollard, 2016) are disabled in the main simulations below, so the future collapse of West Antarctica is relatively slow and driven mainly by sub-ice-shelf oceanic melt and ductile processes as in other models (Feldmann and Levermann, 2015; Golledge et al., 2015; Arthern and Williams, 2017). This provides a better test of the modifications above, without the overall retreat being dominated by more drastic retreat mechanisms.

Fig. ~~7~~ 8 shows the equivalent sea level rise corresponding to net ice melt from West Antarctica, for three types of simulations: (1) control with perpetual modern climate, (2) future RCP8.5 scenario with hydrofracturing and cliff collapse disabled, and (3) future RCP8.5 scenario with those mechanisms enabled. Each simulation is run for the same pair of model versions as for the MISMIP+ and MISMIP3d experiments above: the previous standard version and the new version with the modifications described in section 2.~~same three model versions A, B and C with combinations of the new modifications, as described for the MISMIP+ experiments above.~~

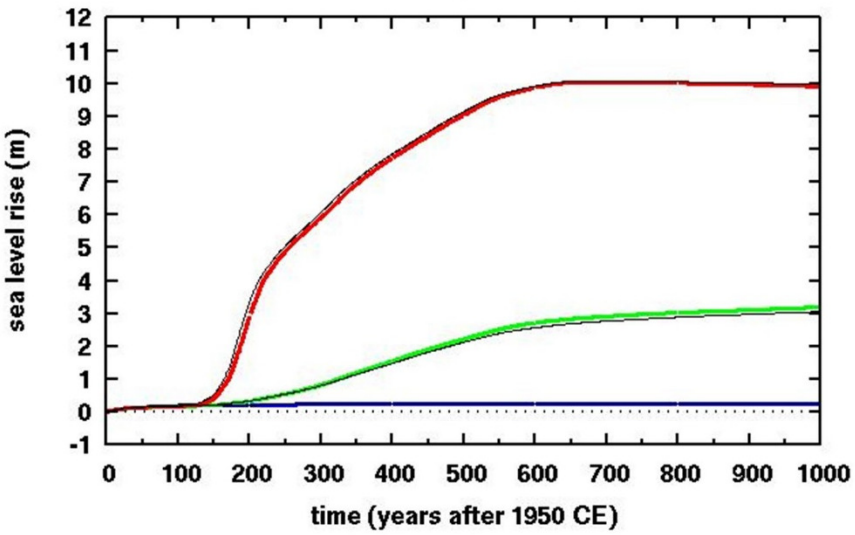

Figure ~~7~~8. Equivalent global sea level rise in simulations of future West Antarctic ice retreat with climate forcing based on the RCP8.5 greenhouse gas scenario. The sea-level rise calculation accounts for ice grounded below sea level, which if melted contributes only its ice-over-flotation amount. ~~**Thin lines:** with previous model (no modifications, version A). **Medium lines:** with new 2-D grounding-line orientation (section 2.1, version B).~~ **Thick colored lines:** n~~with n~~ew~~ew~~ model version.~~2-D orientation and new grid-cell weighting of imposed grounding-line velocities (section 2.2, version C).~~ **Thin black lines:** previous model version. **Blue:** control (perpetual modern climate). **Green:** with ~~with~~ RCP8.5 forcing, without hydrofracturing or cliff failure. **Red:** with RCP8.5 forcing, with hydrofracturing and cliff failure.

As expected, for the future RCP8.5 simulations with no hydrofracturing or cliff failure (type 2), West Antarctic grounding lines retreat deep into the interior over several centuries. After 500 years, nearly all West Antarctic marine ice melts producing ~3 m of sea level rise, similar to that found by the other models noted above. With hydrofracturing and cliff failure enabled (type 3), much more rapid and pervasive grounding-line retreat occurs, with most West Antarctic marine ice melted within ~200 years, as in DeConto and Pollard (2016). In all simulations, the new modifications make very little difference to these results, in contrast to the MISMIP+ fjord-like experiments. Presumably this is due to the larger lateral scales and less influence of lateral boundaries in the major West Antarctic basins, so that the flow in the central regions of these basins is more 1-D (flowline) in character, better represented by the simpler "staircase" grounding-line treatment of the standard model. This is consistent with our results in the ABUMIP intercomparison involving continental Antarctic experiments, where the previous model version was used and results lie within the ranges of the other models (Sun et al, 2020).

Spatial maps of ice distribution and buttressing factor are shown in Figs. ~~8~~ 9 and ~~9~~ 10 for selected times in the future simulation without hydrofracturing or cliff failure (type 2). Except for points right at the grounding line, the buttressing factor θ in Fig. ~~9~~ 10 is purely diagnostic and has no effect on the model physics. Away from the grounding line, θ is calculated for these figures based on stress normal to the direction of ice flow, otherwise following Eqs. (3) to (6b) in section 2~~.1~~ above. There are some differences due to the new modifications, mainly in the ice-shelf interiors for θ away from grounding lines ~~in version A vs. B and C~~), but overall the distributions are similar~~, especially near the grounding lines where θ does enter into the model physics~~. For modern, the θ maps can be compared directly with those in Fürst et al. (2016), who calculated the same quantity (their K_n is our 1 -- θ) from assimilated modern ice-shelf velocities, but using the orientation with minimum N (maximum buttressing) instead of ice flow direction. Even so, t~~T~~he patterns compare favorably with our map~~s~~ for the new ~~modifications~~ model version (Fig. 10b).~~versions B and C).~~

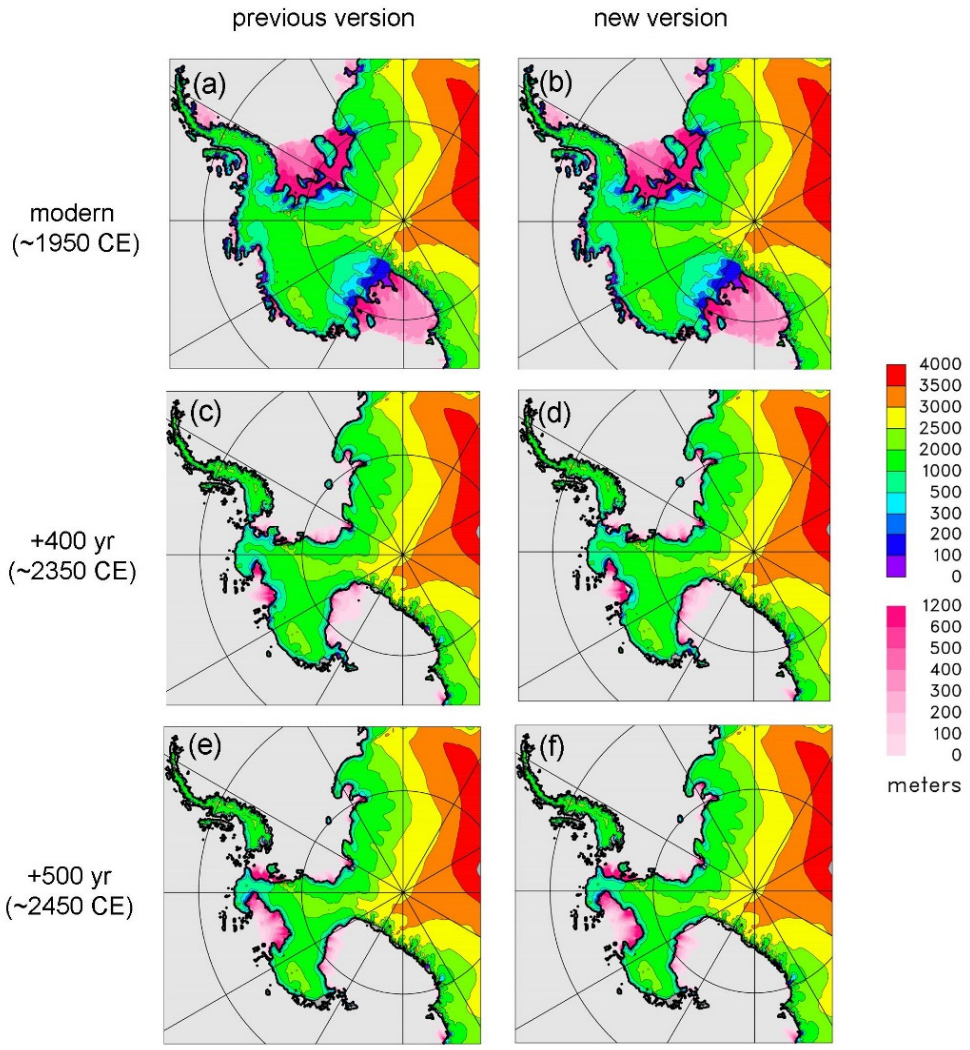

Figure ~~8~~9. Spatial maps of simulated future West Antarctic ice retreat with RCP8.5 forcing, without hydrofracturing or cliff failure, showing grounded ice surface elevations (m, rainbow scale) and floating ice thicknesses (m, pink scale). **1st row (a-~~e~~b):** at year 0 (~1950 CE). **2nd row (~~d f~~c-d):** at year 400 (~2350 CE). **3rd row (e-f~~g i~~):** at year 500 (~2450 CE). **1st column (a,c,~~e~~d,g):** ~~with earlier~~ previous model version ~~(no modifications, version A)~~. **2nd column (b,de,~~f~~h):** ~~with~~ new model version. ~~2-D grounding line orientation (section 2.1, version B).~~ ~~**3rd column (c,f,i):** with new 2-D orientation and new grid-cell weighting of imposed grounding-line velocities (section 2.2, version C).~~

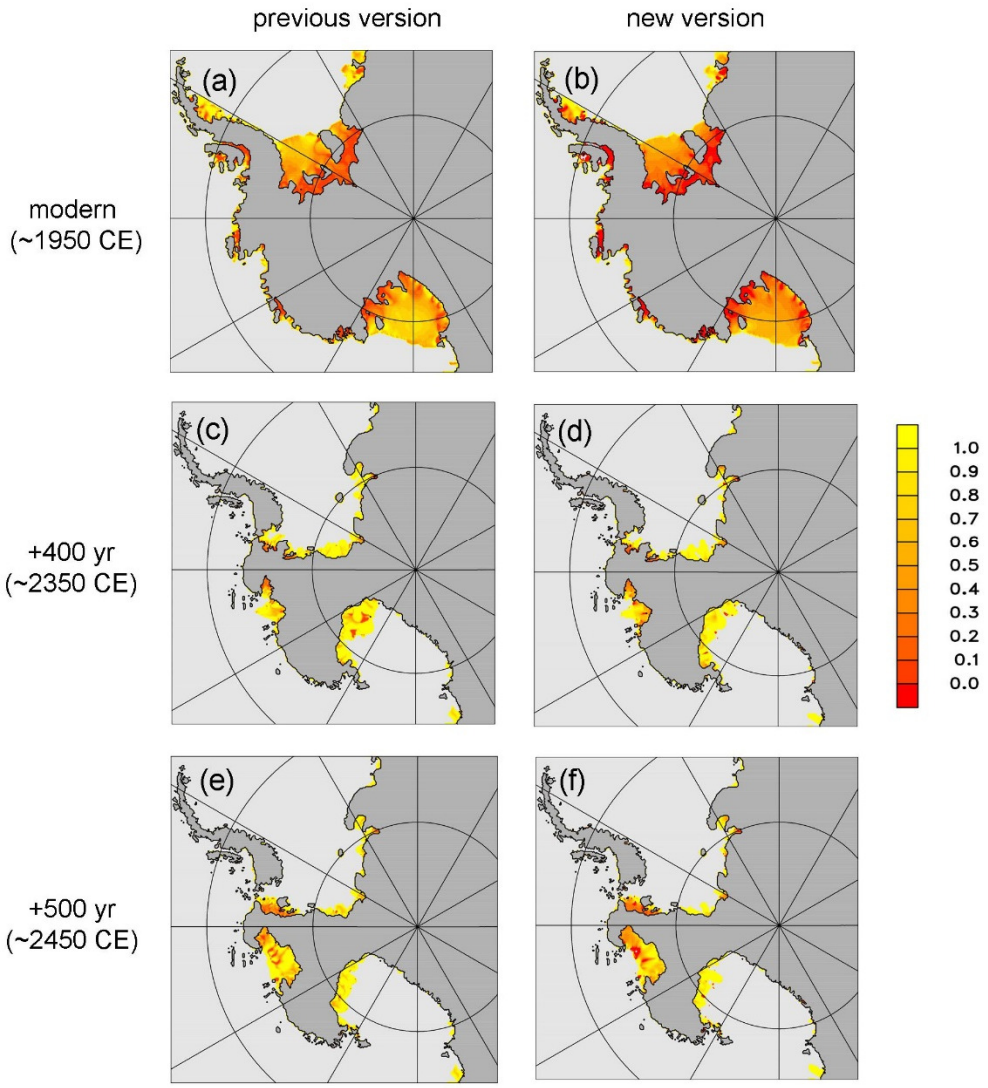

Figure ~~9~~10. As Fig. ~~8~~ 9 showing buttressing factor θ (diagnostic except at grounding line).

~~5~~6. Results: potential for structural failure at West Antarctic grounding lines

As grounding lines retreat across central West Antarctica in the RCP8.5-driven simulations above, they encounter very deep bathymetry with depths of ~1 to 2.5 km below sea level, especially in the Bentley Subglacial Trench (Fig. ~~10~~11). Simple vertically integrated force balance calculations (Bassis and Walker, 2012; Pollard et al., 2015) and vertically resolved modeling (Bassis and Jacobs, 2013; Ma et al., 2017; Schlemm and Levermann, 2019; Benn et al., 2019; Parizek et al, 2019; cf. Clerc et al., 2019) suggest that ice columns at such deep grounding lines, if unbuttressed or only weakly buttressed by ice shelves or mélange, will be structurally unstable, with deviatoric stresses exceeding the material yield stress of the ice. Once initiated, structural "cliff" failure would be expected to propagate extremely rapidly into ice upstream of the grounding line, only stopping when shallower bathymetry is reached, or if buttressing increases somehow.

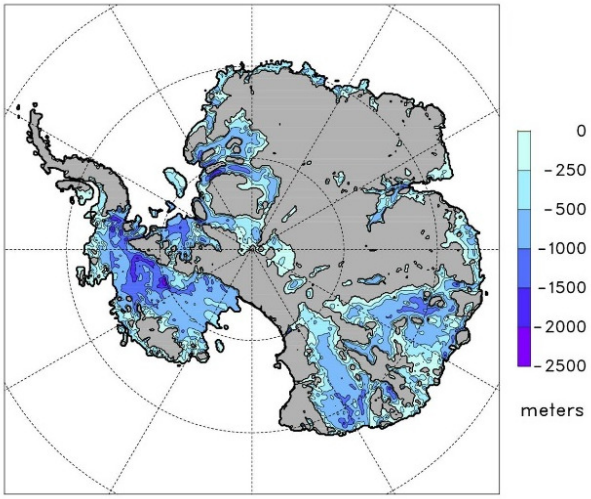

Figure ~~10~~11. Modern observed Antarctic bedrock elevations where below sea level, aggregated to the 10-km model grid from Bedmap2 (Fretwell et al., 2013). As in Fig. 1b of Pollard et al. (2015).

In our simulations without hydrofracturing or cliff failure physics (type 2), structural failure is not part of the model, but we can use the new improved calculations of grounding-line buttressing factors and deviatoric stresses to examine the basic force balance as grounding lines traverse the deep central West Antarctic regions, and so to diagnose if structural failure would occur, or conversely, if it would be prevented by buttressing of ice shelves.

The relevant equation for vertical mean quantities at the grounding line, derived by simple force balance (Bassis and Walker, 2012; Pollard et al, 2015), is:

$$2\,\tau_{x'x'} = \frac{\rho_i(1-\rho_i/\rho_w)gh^2\theta}{2(h-d_s-d_b)} \qquad (11)$$

where $\tau_{x'x'}$ is the depth-averaged normal deviatoric stress at the grounding line (in direction x' to distinguish it from the model's x axis). Note that this applies equally to grounding lines with ice shelves, and to ice cliffs at grounding lines without an ice shelf (for which θ =1). The crevasse depths d_s (surface) and d_b (basal) are Nye-depths as described in section 2.3 above, and depend on principal deviatoric stress. Their sum $d_s + d_s = \theta\, h\, /\, 2$, where h is the ice thickness (Pollard et al., 2015). θ in (11) is from Eq. 6b, using the principal stress direction yielding maximum θ.

~~Assuming~~ With x' i~~ns close to~~ the horizontal principal stress direction, the quantity $2\tau_{x'x'}$ is a good approximation for the difference in the two principal stresses in the $x'$and z plane, which is reported in laboratory experiments as a measure of ice yield strength, typically around ~1 MPa (Bassis and Walker, 2012). Several other considerations may modify this value and the concept of a uniform ice yield strength itself (Parizek et al., 2019; Clerc et al., 2019), including deformation unique to cliffs such as slumping and torques, ice cohesion and modes of failure depending on depth, and importantly, the amount of pre-existing fractures, buried crevasses, bubbly ice and/or cm-scale grain sizes, as opposed to relatively pristine ice with small (~mm-scale) grain sizes. Ice with extensive pre-existing damage is prevalent in most ice cores and presumably throughout Antarctica, and has yield strengths around ~1 MPa, much weaker than pristine ice; Parizek et al. (2019) and Clerc et al. (2019) agree that maximum

heights of subaerial ice cliffs (above sea level, with ~9 times that below sea level) are approximately 100 to 200 m for pre-damaged ice, and ~500 m for pristine ice. In our diagnosis below, we assume that central West Antarctic ice is typically pre-damaged (or if it is not already, it will likely become so as the rapidly retreating grounding line approaches from the north), and so assume an ice yield strength of around ~1 MPa.

In Fig. ~~11~~12, θ and the relevant deviatoric stress measure ($2\tau_{x'x'}$ from Eq. 11) are plotted at grounding lines for the simulation without hydrofracturing or cliff failure (type 2), and with the ~~for the~~ new modifications ~~el~~ in section 2.~~version C with both new modifications.~~ For modern, $2\tau_{x'x'}$ is far below 1 MPa at all grounding lines, as it should be as no significant structural failure is observed today. At +400 years into the run (~2350 CE), when the retreating central West Antarctic grounding lines are beginning to encounter deep (>1 km) bathymetry, the surviving ice shelves shown in Fig. ~~8~~ 9 still provide some buttressing, and most buttressing factors are well below 1; (even though these ice shelves are too short and thin to reach distant pinning points, the lateral curvature in their flow produces back stress). Most $2\tau_{x'x'}$ values are somewhat below 1 MPa, indicating that extensive structural failure is unlikely.

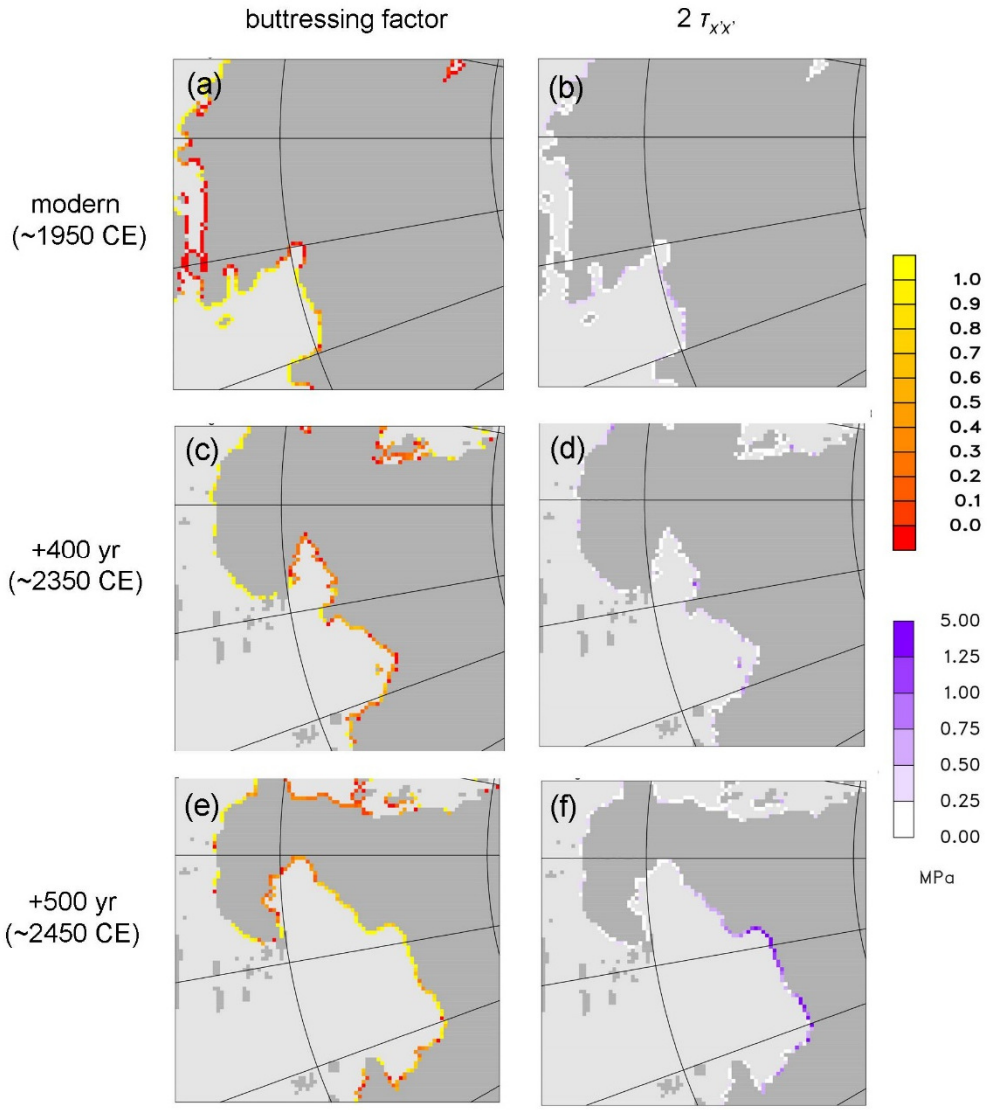

Figure ~~11~~12. Grounding-line quantities in simulated future West Antarctic ice retreat with RCP8.5 forcing, without hydrofracturing or cliff failure, for the new model version ~~version C with both new modifications~~. **1st row (a-b):** at year 0 (~1950 CE). **2nd row (c-d):** at year 400 (~2350 CE). **3rd row (e-f):** at year 500 (~2450 CE). **1st column (a,c,e):** buttressing factor θ at grounding line. **2nd column (b,d,f):** $2\tau_{x'x'}$, where $\tau_{x'x'}$ is the depth-averaged deviatoric normal stress at grounding lines, MPa (Eq. 11). An enlarged subset of the model domain is shown, to better show the grounding-line quantities in the central West Antarctic regions with deep bathymetry.

However, by +500 years (~2450 CE), central West Antarctic grounding lines experience even deeper bathymetry, and many θ values are at or close to 1 (weakly buttressed or essentially unbuttressed). Many $2\tau_{x'x'}$ magnitudes are at or exceed 1 MPa, indicating that structural failure of these grounding-line columns would occur.

~~6~~7. Discussion and Conclusions

The modifications described ~~and tested~~ above ~~in (i) 2-D orientation of the grounding line~~ in calculating the 2-D orientation of the grounding line, i~~the buttressing factor and i~~mposed ~~normal~~ ice flow direction, and buttressing factor~~,~~ ~~and (ii) grid-cell weighting of imposed grounding-line velocities,~~ yield ~~are~~ physically reasonable results. The first modification more ~~rigorously~~ realistically represents the true geometry of the grounding line.

In the idealized fjord-like MISMIP+ and MISMPI3d experiments, which involve strong 2-D curvature of grounding lines in a rectangular channel, the modifications have significant effects on the model's grounding-line variations, bringing them in line with those of other higher-order higher-resolution models in th~~e MISMIP+~~ intercomparisons (Cornford et al., 2020; Pattyn et al., 2013; Patty and Durand, 2013). Best overall intercomparison results are obtained with the buttressing factor at the grounding line based on the maximum extensional stress over all directions (Appendix A).~~This suggest that the modifications are real improvements to the model physics.~~

In contrast, the modifications have relatively little effect in large-scale simulations of future rapid West Antarctic ice retreat. This is presumably because of the larger lateral scales of major West Antarctic basins, so that grounding-line retreat in these basins is more one-dimensional in character, and better represented by the simpler "staircase" grounding-line treatment of the standard model. This is borne out by results of pan-Antarctic experiments in the ABUMIP intercomparison (Sun et al., 2020), which lie within the range of the other models.

The ~~more rigorous~~ improved treatments of grounding-line orientation and buttressing factor~~s~~ allow us to better diagnose the force balance at grounding lines in the West Antarctic simulations, to see if structural failure could occur in a future with unmitigated greenhouse-gas warming. We find that when grounding lines reach very deep central West Antarctic regions (~1 to 2.5 km below sea level) after about 500 years, ice-shelf buttressing is weak and the deviatoric stress measures widely exceed the ice yield stress, implying that structural failure would occur at these grounding lines. In that case, a runaway disintegration could be initiated, with structural failure propagating very rapidly into the remaining grounded ice (Schlemm and Levermann, 2019), which in the absence of renewed buttressing would continue until shallower bathymetry is reached to the south.

Several other ice sheet-shelf models have performed similar projections of future West Antarctic retreat (e.g., Feldmann and Levermann, 2015; Golledge et al., 2015; Arthern and Williams, 2017), some with higher order and/or higher resolution than

ours. We suggest it would be beneficial to examine these grounding-line quantities in other model simulations, to more robustly assess the danger of structural failure in future centuries under RCP8.5-like climate warming.

Apart from ice shelves, another potential source of buttressing is from mélange. Huge amounts of floating ice debris (mélange) would be generated in front of the retreating ice fronts in the above scenarios. In major Greenland fjords today such as Jakobshavn and Helheim, mélange is considered to provide significant back stress on the glacier calving front, at least in winter (e.g., Burton et al., 2018). However, in one study using a heuristic continuum model of mélange (Pollard et al., 2018), its back stress on ice shelves and grounding lines is negligible during West Antarctic retreat. In contrast to the narrow Greenland fjords, mélange in the much wider West Antarctic embayments flows northward into the Southern oceans nearly unimpeded.

Other processes that could reduce the deep bathymetry encountered by future grounding lines are bedrock rebound under the reduced ice load, and less gravitational attraction of the ocean by the receding ice (Gomez et al., 2015). The West Antarctic simulations here include the first process, using a relatively simple ELRA (Elastic Lithosphere Relaxing Asthenosphere) bed model (Pollard and DeConto, 2012), and the rebound of the modern bathymetry (Fig. ~~10~~11) under the central grounding lines after 400 to 500 years (Fig. ~~11~~12) is minor. However, recent geophysical data indicate very low mantle viscosities below parts of West Antarctica (Heeszel et al., 2016; Barletta et al., 2018), which could produce faster rebound and shallower bathymetry by the time grounding lines retreat into central regions. Work to develop Earth-sea level models with laterally varying properties and ice-ocean gravitational interaction, and couple them with ice-sheet models, is ongoing (Gomez et al., 2018; Powell et al., 2020).

Appendix A. Variations in calculating θ

For all new-model results in the main paper, the buttressing factor θ is given by Eq. (6b), in which the deviatoric normal stress at the grounding line is given by N_{max}, its maximum extensional (principal stress) value over all possible directions 0 to 360° in Eq. (4). It is a good approximation in the central part of fjord-like channels (Gudmundsson, 2013, Fig. 1); in the shearing margins with stronger buttressing, the resulting θ values still agree reasonably (ibid; his Fig. 2 vs. our Fig. 5). As shown below, this method yields better overall MISMIP+ and MISMIP3d results than all alternatives tried, including simply using the grounding-line normal (n_x,n_y) in Eq. (4) and (6a). We suspect this is because during retreat of an otherwise uniform grounding line in our model, unavoidably there are isolated single grid-cell changes from grounded to floating to ice at each timestep. This produces temporary zig-zags in the grounding line that are not completely muted by the orientation algorithm, and cause spurious single-cell distortions of the flow and overall retreat if θ is given by (6a), which are avoided if θ is given by (6b). However, we emphasize that the latter method was chosen for the main paper not because of the above rationale, but because it yields the best overall intercomparison results.

Several alternate methods of determining θ are described below, and results are compared with the method using N_{max} and Eq. (6b) as in the main paper. These alternatives stem from the inherent uncertainty in using a 1-D flowline parameterization (Eq. 1) within a 2-D model. Uncertainties in estimating θ in numerical models are also discussed in Gudmundsson (2013). The four alternate methods for calculating N in Eq. (4) and hence θ in Eq. (6) are as follows, labelled A to D:

E. Using the direction (n_x,n_y) normal to the grounding line given by the new orientation algorithm in section 2.

F. Using the direction of ice flow from the preliminary grid-solution (u,v) (these velocities are also used in Eq. 5).

G. Using maximum N over all directions (Eq. 6b) as in the main paper, but with the strain rates in Eq. (5) calculated for the first ice shelf cell that is entirely surrounded by other ice-shelf cells, searching along a trajectory (n_x,n_y) normal to the grounding line. This avoids "contaminating" the strain rates with velocity points within grounded ice, especially for ice-shelf cells with up to 3 neighboring grounded-ice cells.

H. Using maximum N over all directions (Eq. 6b) as in the main paper, but with the parameterized speed U_g in (1) applied in the direction normal to the grounding line (n_x,n_y), and with the component parallel to the grounding line equal to that of the preliminary grid-solution (cf., Gudmundsson, 2013, Fig. 1).

MISMIP+ and MISMIP3d results for all four methods are shown in Fig. A1. For comparison, thin black lines in each panel show results for the method used in the main paper (Eq. 6b). For MISMIP+, methods A and B yield similar results to the main paper, all within the shaded ranges of the other models. Method C diverges drastically for the Ice1 experiment (Fig. A1c), and method D is nearly outside the range for the Ice2 experiment (Fig. A1h).

For MISMIP3d, methods A and B yield poor results similar to our original MISMIP3d experiments, with considerably larger grounding-line excursions and quite different total changes than the other models. Methods C and D yield almost the same results as the main paper, much closer or within the other model ranges. Hence all four alternate methods A-D yield results that are poorer than that in the main paper, for at least one of the MISMIP+ and MISMIP3d experiments.

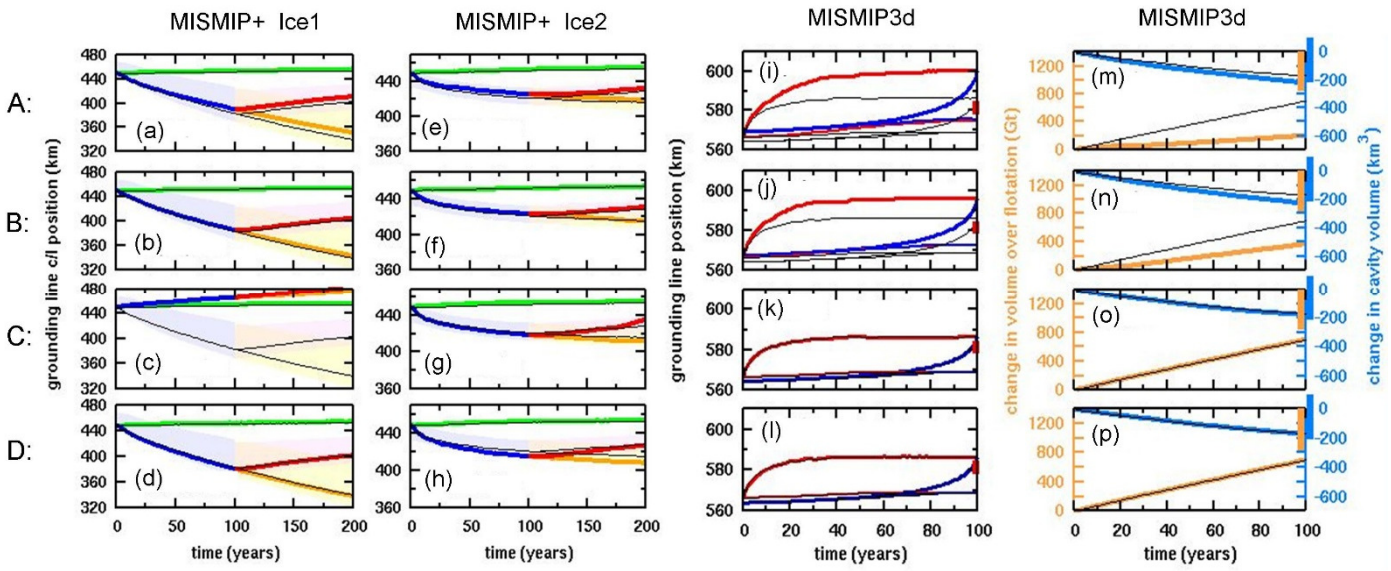

Figure A1. MISMIP+ and MISMIP3d results for four alternate methods of determining buttressing factor θ. **Rows (top to bottom)** are for methods A to D described in the text. **Column (a-d):** MISMIP+ Ice1 experiment, as in Fig. 3. **Column (e-h):** MISMIP+ Ice2 experiment, as in Fig. 6. **Column (i-l):** MISMIP3d experiment, grounding-line positions as in Fig. 7a. **Column (m-p):** MISMIP3d experiment, changes in total volume over flotation and cavity volume as in Fig. 7b. **Thick colored lines:** as in the main paper except with one of the alternate θ methods. **Thin black lines:** as in the main paper with the new θ method described in section 2 using Eq. (6b).

Fig. A2 shows simulations of future West Antarctic retreat, for all four alternate θ methods described above. The alternate methods have very little effect on equivalent sea-level rise, as also seen for the new vs. previous method in the main paper (Fig. 8); again this is presumably due to the more one-dimensional character of ice retreat in major Antarctic basins, with wider lateral scales than the MISMIP+ and MISMIP3d channels.

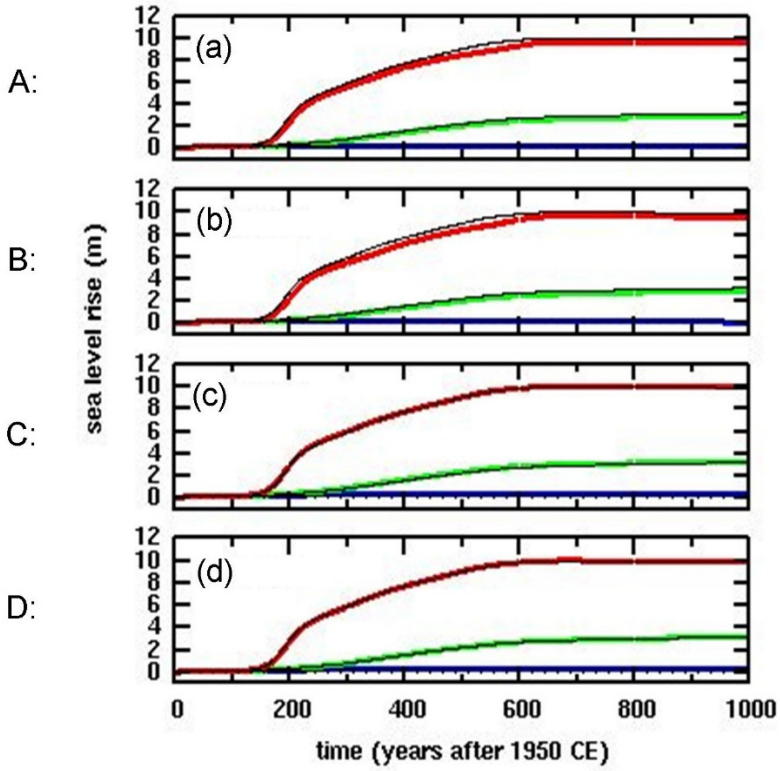

Figure A2. Equivalent global sea level rise in simulations of future West Antarctic ice retreat with climate forcing based on RCP8.5 greenhouse-gas scenario. **(a) to (d):** with the four alternate θ methods A to D described in the text. **Thick colored lines**: as in the main paper except with one of the alternate θ methods. **Thin black lines:** as in the main paper with the new θ method described in section 2. **Blue:** control (perpetual modern climate). **Green:** with RCP8.5 forcing, without hydrofracturing or cliff failure. **Red:** with RCP8.5 forcing, with hydrofracturing and cliff failure.

Appendix B. Speculative modifications in grounding-line flux parameterization

Going beyond Schoof (2007), a few recent analytical studies have investigated aspects of boundary-layer treatments of grounding-line zones ~~,~~ (Reese et al., 2018; Haseloff and Sergienko, 2018; Sergienko and Wingham, 2019)~~, such as Haseloff and Sergienko (2018) and Sergienko and Wingham (2019).~~ Here we briefly test three~~wo~~ modifications to our grounding-line flux implementation that are more heuristic and speculative than those in the main paper. They are roughly motivated by the recent studies~~work~~ although they cannot represent ~~i~~them~~t~~ directly ~~and address different aspects~~.

B1. Strong buttressing

If the buttressing factor θ given by (6) falls to zero or below, this corresponds to compressive horizontal deviatoric stress normal to the grounding line, and compressive (negative) strain in the direction of flow. However, its use in the Schoof formation (1) for grounding-line ice velocity U_g unrealistically predicts very small or zero U_g as θ falls to zero. (Eq. (1a) would be invalid for $\theta <$ 0, as noted by Reese et al. (2018); for this equation we reset θ to be within the range [0,1] as mentioned in section 2). This does not occur extensively in our simulations of future Antarctic retreat, because buttressing is generally small as grounding lines rapidly recede into wide interior basins, and is more of a concern in colder climates with expanded grounding lines and shelf ice.

To crudely assess the problem, the value of θ in Eq. (1a) is adjusted for small values so that it does not fall exactly to 0.

If $\theta < 0.3$, then $\theta' = \theta + 0.15\,((0.3 - \theta)/0.3\,)^2$ (B1)

(This is applied after θ is reset to the range [0,1] for Eq. (1a)). The adjusted value θ' falls only to 0.15 for strong buttressing, allowing small but non-zero flux. This does not rigorously address the problem, but can provide a guide to its severity by its effect on results.

~~A1~~B2. Strain softening

This modification addresses the presumed underestimate of strain softening in the grounding zone in a purely 1-D flowline treatment such as Schoof (2007). With no lateral variations, the second invariant of the horizontal strain tensor, entering in ice viscosity in the SSA equations, is

$$\dot{\varepsilon}_{1D}{}^2 = (\partial u/\partial x)^2 \qquad (~~A1~~B2)$$

as in Schoof (2007). With lateral variations and two-dimensional flow, it is

$$\dot{\varepsilon}_{2D}{}^2 = (\partial u/\partial x)^2 + (\partial v/\partial y)^2 + (\partial u/\partial x)(\partial v/\partial y) + \tfrac{1}{4}(\partial u/\partial y + \partial v/\partial x)^2 \qquad (~~A2~~B3)$$

Then the ice viscosity η is

$$\eta = \frac{1}{2\,A^{1/n}\,\dot{\varepsilon}^{(n-1)/n}} \qquad (~~A3~~B4)$$

(e.g., Thoma et al., 2014), where $\dot{\varepsilon}$ is either $\dot{\varepsilon}_{1D}$ or $\dot{\varepsilon}_{2D}$, and A and n are the rheological coefficient and exponent respectively appearing in the Schoof formula Eq. 1a. In our implementation ~~η~~ Eq. (B2) and (B3) are~~is~~ computed using the velocity solution of the previous iteration (Pollard and DeConto, 2012), at the last grounded cell adjacent to the grounding line.

η does not enter in Eq. (1a), but we attempt to compensate for the absence of the 2-D strain-softening in (~~A3~~B4) by altering A in Eq. (1a) by an appropriate factor:

$$A' = A\left(\frac{\dot{\varepsilon}_{2D}}{\dot{\varepsilon}_{1D}}\right)^{n-1} \qquad (\text{~~A4~~B5})$$

This is not rigorous because the Schoof analysis incorporates the 1-D dependence (~~A1~~B2) in its derivation, and not (~~A2~~B3). However the modification to A in (~~A4~~B5) is at least in the right direction (increasing the ice flux across the grounding line), and may be useful as a crude approximation.

~~A2~~B3. Overestimate of ice flux for high basal sliding coefficients

Sergienko and Wingham (2019) found that in ice streams with high basal sliding coefficients, the boundary-layer expansion of Schoof (2007) is not valid, and can overestimate the flux of ice across the grounding zone. Following on from that paper, the ratio of the newly calculated flux to the Schoof-calculated flux, in idealized tests for small basal slopes, ranges from ~0.6 to 1 but can be much smaller for steeper slopes (O. Sergienko, personal communication, 2020). This analysis cannot be represented by modifications in our model. However, we can crudely estimate the possible effect of such changes for small basal slopes at least, by simply reducing all imposed grounding-line velocities in (1) by a constant factor, i.e., multiplying U_g given by (1b) by a factor 0.6.

~~A3~~B4. Effects on results

The effects of applying each of the modifications described above are shown here. Fig~~s~~. ~~A1~~ B1 ~~and A2~~ shows results for the MISMIP+ Ice1 ~~and Ice2~~ experiment~~s respectively~~, where the effects are similar in magnitude to those shown in the main paper (Figs. 3~~ and 6~~) ~~due to the modifications there~~. By and large, the grounding-line excursions here are still within in the envelopes of other models in the MISMIP+ intercomparison (Cornford et al, 2020).

For the small-θ modification (section B1, Fig. B1a), the differences from the main-paper results are negligible, implying that the shortcomings of the flux parameterization (Eq. 1a) for strong buttressing do not have a large effect on grounding-line migration, at least in fjord-like scenarios. The reason may be that in regions of strong buttressing near the margins, grounding-line fluxes are relatively small, and allowing them to be zero has little effect on the overall evolution (consistent with Gudmundsson, 2013, Fig. 4). For the strain-softening modification (section B2, Fig. B1b), there is a serious degradation in results, which now are near the outer edges of the other model envelopes and exhibit spurious fluctuations, indicating this modification is not viable. For the 0.6 U_g modification (section B3, Fig. B1c), the results are at least as good as in the main paper, implying that grounding-line migration is not extremely sensitive to uniform changes in the magnitude of the parameterized flux in Eq. (1a).

~~The "sign" of the two effects in these figures is as follows: if the modification basically increases (decreases) the imposed grounding line flux, the rates and amplitudes of the grounding line variations increase (decrease). The strain-softening modification in section A1 has the former effect (increased flux, increased response), and the U_g modification in section A2 has the latter effect (decreased flux, decreased response).~~

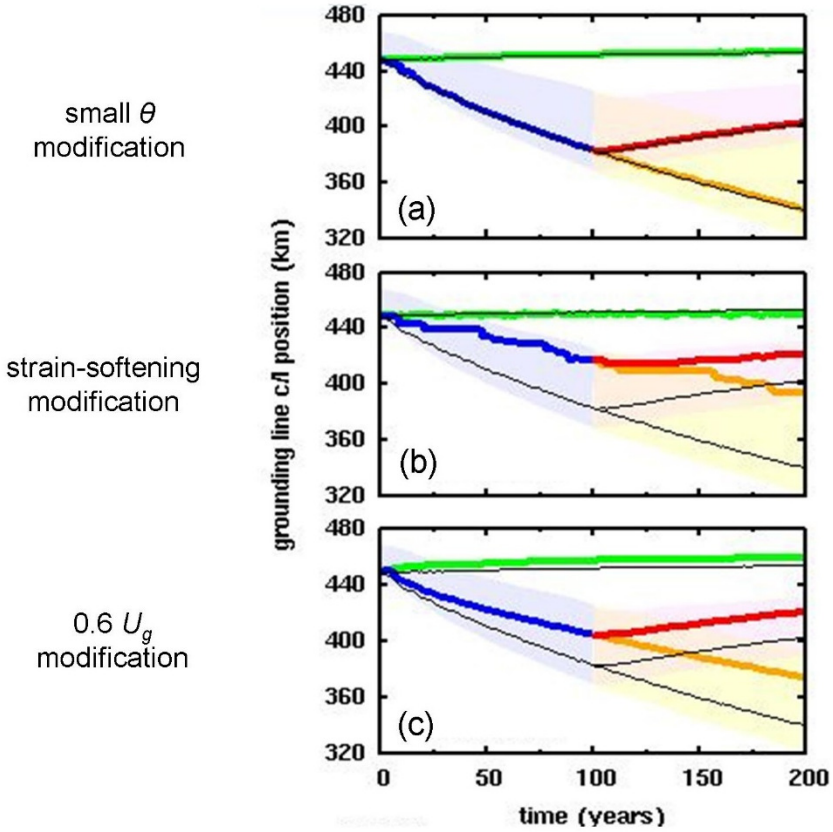

Figure ~~A1~~B1. Along-fjord centerline position (km) of grounding lines in the MISMIP+ Ice1 experiment (Cornford et al., 2020). **(a)** with small-θ modification described in section B1. **(b)** with strain-softening modification described in section B2. **(c)** with 0.6 U_g modification described in section B3. **Thick colored lines:** ~~with new modifications~~ as in main paper except with one of the above modifications ~~(model version C)~~. **Thin black lines:** as in main paper with no further modification.~~model version C and strain-softening modification in section A1. **Crosses:** model version C and U_g modification in section A2.~~ **Green:** control (continuation of spin-up with zero oceanic melt). **Blue and yellow:** with oceanic melt perturbation. **Red:** with oceanic melt reset zero after year 100. Shaded regions show the envelopes for the "main subset" of MISMIP+ models, copied from Cornford et al. (2020, their Fig. 7a).

Fig. ~~A3~~ B2 shows results for future West Antarctic retreat, for simulations without hydrofracturing or cliff failure. All three~~The~~ modifications ~~in the Appendix~~ described above have very little effects on equivalent sea-level rise, as was also seen ~~for the modifications~~ in the main paper (Fig. ~~7~~8); again this is presumably due to the more one-dimensional character of ice retreat in major Antarctic basins, which have~~ith~~ wider lateral scales than the ~~narrow~~ MISMIP+ and MISMIP3d channels.

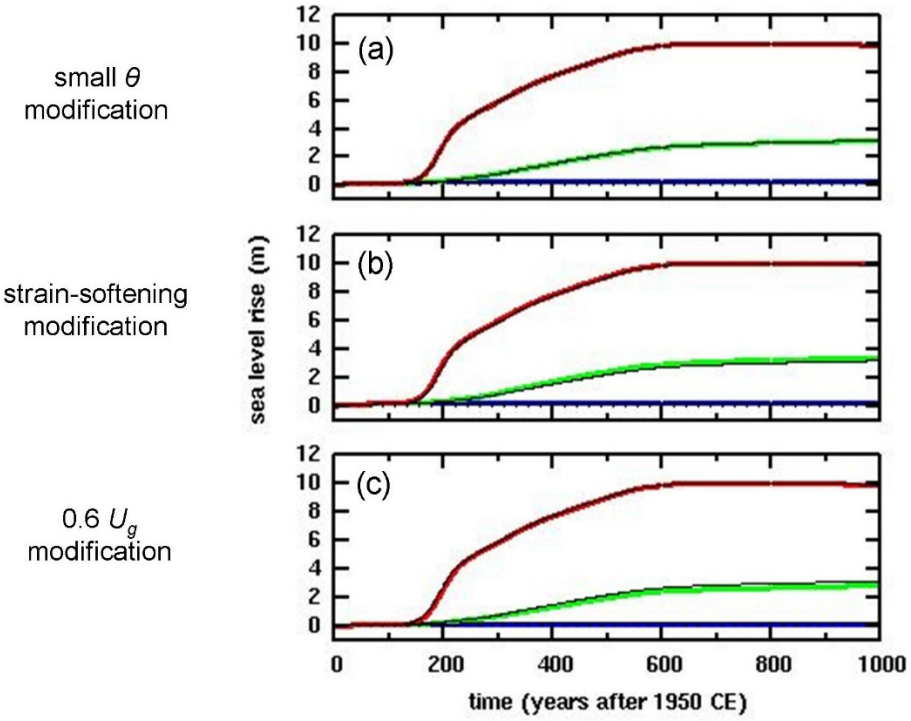

Figure ~~A3~~B2. Equivalent global sea level rise in simulations of future West Antarctic ice retreat with climate forcing based on RCP8.5 greenhouse-gas scenario. **(a)** with small-θ modification described in section B1. **(b)** with strain-softening modification described in section B2**.** **(c)** with 0.6 U_g modification described in section B3**.** ~~**Thick lines:** with new modifications in main paper (model version C)~~**Thick colored lines:** as in main paper except with one of the above modifications. **Thin black lines:** as in main paper with no further modification~~**Medium lines:** model version C and strain-softening modification in section A1. **Thin lines:** model version C and U_g modification in section A2~~. **Blue:** control (perpetual modern climate). **Green:** with RCP8.5 forcing, without hydrofracturing or cliff failure. **Red:** with RCP8.5 forcing, with hydrofracturing and cliff failure.

Appendix C. Calculation of crevasse depths

For all runs in this paper, an improvement is made in the parameterization of crevasse depths, used both in "normal" calving and also in the cliff-failure physics (Pollard and et al., 2015). Crevasse depths are set to the Nye-depth (at which total horizontal stress is zero for surface crevasses, or is equal to water pressure for basal crevasses; Nye, 1957; Jezek, 1984; Nick et al., 2010). Previously, the divergence ($\partial u/\partial x + \partial v/\partial y$) was used along with ice viscosity as a simple estimate of the horizontal deviatoric stress (Pollard et al., 2015). Here, this is replaced by the maximum principal deviatoric stress (Turcotte and Schubert, 1982), calculated from the strain rates and viscosity. This is a small improvement "in principle". It has no effect in the idealized fjord MISMIP+ and MISMIP3d experiments for which calving is disabled, and has negligible effect in the West Antarctic simulations as shown in Fig. C1.

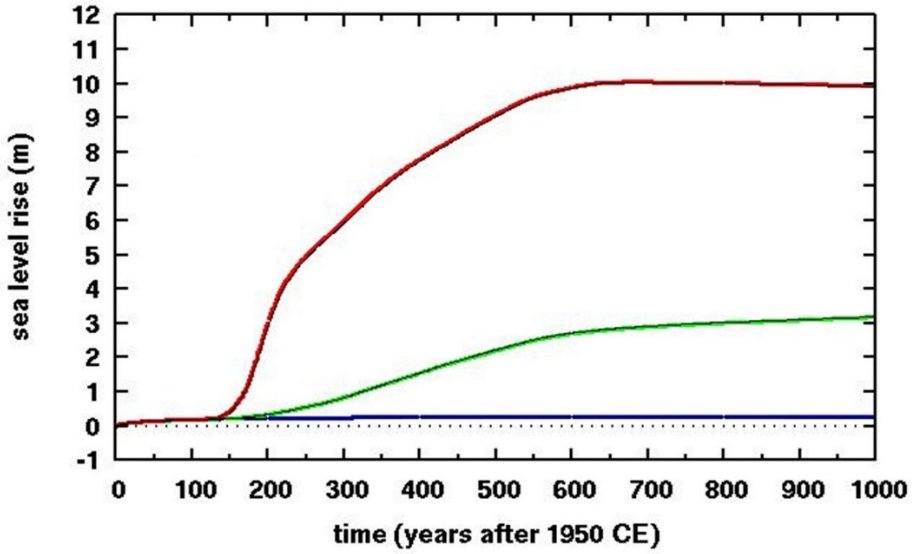

Figure C1. Equivalent global sea level rise in simulations of future West Antarctic ice retreat with climate forcing based on RCP8.5 greenhouse-gas scenario. **Thick colored lines:** as in main paper except with the previous parameterization of crevasse depths based on divergence. **Thin black lines:** as in the main paper (which includes the new crevasse-depth parameterization). **Blue:** control (perpetual modern climate). **Green:** with RCP8.5 forcing, without hydrofracturing or cliff failure. **Red:** with RCP8.5 forcing, with hydrofracturing and cliff failure.

~~*Code and Output Availability.* The ice sheet model code is available on request from the corresponding author (pollard@essc.psu.edu). That and selected model output will be available at Penn State's Data Commons, .~~

Code and data availability. Selected output files, metadata and model code are available on Penn State's Data Commons archive at http://www.datacommons.psu.edu/commonswizard/MetadataDisplay.aspx?Dataset=6238, and at https://doi.org/10.26208/m3bt-jy63.

Author contributions. DP and RD conceived the project and design. DP performed coding and simulations and wrote the manuscript with input from RD.

Competing interests. The authors declare that they have no conflict of interest.

Acknowledgements. This work was supported by US National Science Foundation grant NSF ICER-1663693 and National Aeronautics and Space Administration grant NASA NNH16ZDA001N-SLCST. We thank Richard Alley for helpful advice on the discussion of ice yield stress in section ~~5~~6, and reviewers Frank Pattyn and Stephen Cornford for insightful comments and suggestions.

References

Arthern, R.J. and Williams, C.R.: The sensitivity of West Antarctica to the submarine melting feedback. Geophys. Res. Lett., 44, 252-2359, 2017.

Barletta, V.R., Bevis, M., Smith, B.E., Wilson, T., Brown, A., Bordoni, A., Willis, M., Abbas Khan, S., Rovira-Navarro, M., Dalziel, I., Smalley Jr., R., Kendrick, E., Konfal, S., Caccamise II, D.J., Aster, R.C., Nyblade, A., and Wiens, D.A.: Observed rapid bedrock uplift in Amundsen Sea Embayment promotes ice-sheet stability. Science, 360, 1335-1339, 2018.

Bassis, J.N. and Walker, C.C.: Upper and lower limits on the stability of calving glaciers from the yield strength envelope of ice. Proc. Roy. Soc. A, 468, 913-931, 2012.

Bassis, J.N. and Jacobs, S.: Diverse calving patterns linked to glacier geometry. Nature Geosci., 6, 833-836, 2013.

Benn, D., Åström, J., Zwinger, T., Todd, J., and Crawford, A.: Marine ice-cliff instability: How does it work, and what controls ice retreat rates? Geophysical Research Abstracts Vol. 21, EGU2019-15396, EGU General Assembly, Vienna, Austria, 2019.

Bueler, E. and Brown, J.: Shallow shelf approximation as a "sliding law" in a thermomechanically coupled ice sheet model. J. Geophys. Res, 114, F03008, doi:10.1029/2008JF001179, 2009.

Burton, J.C., Amundson, J.M., Cassotto, R., Kuo, C.-C., and Dennin, M.: Quantifying flow and stress in ice mélange, the world's largest granular material. Proc. Nat. Acad. Sci., 105, 5105-5110, 2018.

Clerc, F., Minchew, B.M., and Behn, M.D.: Marine ice cliff instability mitigated by slow removal of ice shelves. Geophys. Res. Lett., 46, 12108-12116, 2019.

Cornford, S.L., Martin, D.F., Graves, D.T., Ranken, D.F., Le Brocq, A.M., Gladstone, R.M., Payne, A.J., Ng, E.G., and Lipscomb, W.H.: Adaptive mesh, finite volume modeling of marine ice sheets, J. Comput. Phys., 232, 529–549, doi:10.1016/j.jcp.2012.08.037, 2013.

Cornford, S.L, Martin, D.F., Payne, A.J., Ng, E.G., Le Brocq, A.M., Gladstone, R.M., Edwards, T.L., Shannon, S.R., Agosta, C., van den Broeke, M.R., Hellmer, H.H., Krinner, G., Ligtenberg, S.R.M., Timmermann, R., and Vaughan, D.G.: Century-scale simulations of the response of the West Antarctic Ice Sheet to a warming climate. The Cryo., 9., 1579-1600, 2015.

Cornford, S.L., Martni, D.F., Lee, V., Payne, A.J., and Ng, E.G.: Adaptive mesh refinement versus subgrid friction interpolation in simulations of Antarctic ice dynamics., Ann. Glaciol., 57, doi: 10.1017/aog.2016.132016, 2016.

Cornford, S.L., Seroussi, H., Asay-Davis, X.S., Gudmundsson, G.H., Arthern, R., Borstad, C., Christmann, J., dos Santos, T.D., Feldmann, J., Goldberg, D., Hoffman, M.J., Humbert, A., Kleiner, T., Leguy, G., Lipscomb, W.H., Merino, N., Durand, G., Morlighem, M., Pollard, D., Rückamp, M., Williams, C.R., and Yu, H.: Results of the third Marine Ice Sheet Model Intercomparison Project (MISMIP+), ~~The Cryo. Disc., https://doi.org/10.5194/tc-2019-326, 2020.~~The Cryo., 14, 2283-2301, 2020.

DeConto, R.M. and Pollard, D.: Contribution of Antarctica to past and future sea-level rise. Nature, 531, 591-597, 2016.

Docquier, D., Perichon, L., and Pattyn, F.: Representing grounding line dynamics in numerical ice sheet models: recent advances and outlook, Surv. Geophys., 32, 417-435, 2011.

Drouet, A.S., Docquier, D., Durand, D., Hindmarsh, R., Pattyn, F., Gagliardini, O., and Zwinger, T.: Grounding line transient response in marine ice sheet models. The Cryo., 7, 395–406, 2013.

Feldmann, J. and Levermann, A.: Collapse of the West Antarctic Ice Sheet after local destabilization of the Amundsen Basin. Proc. Nat. Acad., 112, 14191-14196, 2015.

Fretwell, P., et al.: Bedmap2: improved ice bed, surface and thickness datasets for Antarctica. The Cryosphere, 7, 375-393, 2013.

Fürst, J.J., Durand, G., Gillet-Chaulet, F., Tavard, L., Rankl, M., Braun, M., and Gagliardini, O.: The safety band of Antarctic ice shelves. Nature Clim. Change, 6, 479-482, 2016.

Gladstone, R.M., Lee, V., Vieli, A., and Payne, A.J.: Grounding line migration in an adaptive mesh ice sheet model. J. Geophys. Res., 115, F04014, doi:10.1029/2009JF001615, 2010.

Gladstone, R.M., Payne, A.J., and Cornford, S.L.: Resolution requirements for grounding-line modelling: sensitivity to basal drag and ice-shelf buttressing. Ann. Glaciol., 53, 97-105, 2012.

Golledge, N.R., Kowalewski, D.E., Naish, T.R., Levy, R.H., Fogwill, C.J., and Gasson, E.G.W.: The multi-millennial Antarctic commitment to future sea-level rise. Nature, 526, 421-425. 2015.

Gomez, N., Pollard, D., and Holland, D.: Sea-level feedback lowers projections of future Antarctic Ice-Sheet mass loss. Nature Commun., 6, 8798, doi:10.1038/ncomms/9798, 2015.

Gomez, N., Latychev, K., and Pollard, D.: A coupled ice sheet-sea level model incorporating 3D Earth structure: Variations in Antarctica during the last deglacial retreat. J. Climate, 31, 4041-4054, 2018.

Gudmundsson, G.H.: Ice-shelf buttressing and the stability of marine ice sheets. The Cryo., 7, 647-655, 2013.

Haseloff, M. and Sergienko, O.V.: The effect of buttressing on grounding line dynamics. J. Glaciol., 64, 417-431, 2018.

Heeszel, D.S., Wiens, D.A., Anandakrishnan, S., Aster, R.C., Dalziel, I.W.D., Huerta, A.D., Nyblade, A.A., Wilson, T.J., and Winberry, J.P.: Upper mantle structure of the central and West Antarctica from array analysis of Rayleigh wave phase velocities. J. Geophys. Res. Solid Earth, 121, 1758-1775, 2016.

Jezek, K.C.: A modified theory of bottom crevasses used as a means for measuring the buttressing effect of ice shelves on inland ice sheets. J. Geophys. Res., 89, 1925-1931, 1984.

Ma, Y., Tripathy, C.S., and Bassis, J.N.: Bounds on the calving cliff height of marine terminating glaciers. Geophys. Res. Lett., 44, 1369-1375, 2017.

Nick, F.M., van der Veen, C.J., Vieli, A., and Benn, D.I.: A physically based calving model applied to marine outlet glaciers and implications for the glacier dynamics. J. Glaciol., 56, 781-794, 2010.

Nye, J.F.: The distribution of stress and velocity in glaciers and ice sheets. Proc. Roy. Soc. A, 239, 113-133, 1957.

Parizek, B.R, Christianson, K., Alley, R.B., Voytenko, D., Vaňková, I., Dixon, T.H., Walker, R.T., and Holland, D.M.: Ice-cliff failure via retrogressive slumping. Geology, 47, 449-452, 2019.

Pattyn, F., Schoof, C., Perichon, L., Hindmarsh, R.C.A., Bueler, E., de Fleurian, B., Durand, G., Gagliardini, O., Gladstone, R., Goldberg, D., Gudmundsson, G.H., Huybrechts, P., Lee, V., Nick, F.M., Payne, A.J., Pollard, D., Rybak, O., Saito, F., and Vieli, A.: Results of the Marine Ice Sheet Model Intercomparison Project, MISMIP. The Cryo., 6, 573–588, 2012.

Pattyn, F. and Durand, G.: Why marine ice sheet model predictions may diverge in estimating future sea level rise. Geophys. Res. Lett., 40, 4316-4320, 2013.

Pattyn, F., Perichon, L., Durand, G., Favier, L., Gagliardini, O., Hindmarsh, R.C.A., Zwinger, T., Albrecht, T., Cornford, S., Docquier, D., Fürst, J.J., Goldberg, D., Gudmundsson, G.H., Humbert, A., Hütten, M., Huybrechts, P., Jouvet, G., Kleiner, T., Larour, E., Martin, D., Morlighem, M., Payne, A.J., Pollard, D., Rückamp, M., Rybak, O., Seroussi, H., Thoma, M., and Wilkens, N.: Grounding-line migration in plan-view marine ice-sheet models: Results of the ice2sea MISMIP3d Intercomparison. J. Glaciol., 59, 410-422, 2013.

Pollard, D. and DeConto, R.M.: Description of a hybrid ice sheet-shelf model, and application to Antarctica. Geosci. Model Devel., 5, 1273-1295, 2012.

Pollard, D., DeConto, R.M., and Alley, R.B.: Potential Antarctic Ice Sheet retreat driven by hydrofracturing and ice cliff failure. Earth Plan. Sci. Lett., 412, 112-121, 2015.

Pollard, D., DeConto, R.M., and Alley, R.B.: A continuum model (PSUMEL1) of ice mélange and its role during retreat of the Antarctic Ice Sheet. Geosci. Model Devel., 11, 5149-5172, 2018.

Powell, E., Gomez, N., Hay, C., Latychev, K., and Mitrovica, J.X.: Viscous effects in the solid Earth response to modern Antarctic ice mass flux: Implications for geodetic studies of WAIS stability in a warming world. J. Clim., 33, 443-459, 2020.

Reese, R., Winkelmann, R. and Gudmundsson, H.: Grounding-line flux formula applied as a flux condition in numerical simulations fails for buttressed Antarctic ice streams. The Cryosphere, 12, 3229-3242, 2018.

Schlemm, T. and Levermann, A.: A simple stress-based cliff-calving law. The Cryo., 13, 2475-2488, 2019.

Schoof, C.: Ice sheet grounding line dynamics: steady states, stability, and hysteresis. J. Geophys. Res. - Earth Surf., 112, F03S28, doi: 10.1029/2006JF000664, 2007.

Seddik, H., Greve, R., Zwinger, T., Gillet-Chaulet, F., and Gagliardini, O.: Simulations of the Greenland ice sheet 100 years into the future with the full Stokes model Elmer/Ice. J. Glaciol., 58, 427-440, 2012.

Sergienko, O.V. and Wingham, D.J.: Grounding line stability in a regime of low driving and basal stresses. J. Glaciol., 65, 833-849, 2019.

Shields, C.A., Kiehl, J.T., and Meehl, G.A.: Future changes in regional precipitation simulated by a half-degree coupled climate model: Sensitivity to horizontal resolution. J. Adv. Model. Earth Syst., 8, 863-884, 2016.

Sun, S., Pattyn, F., Simon, E.G., Albrecht, T., Cornford, S., Calov, R., Dumas, C., Gillet-Chaulet, F., Goelzer, H., Golledge, N.R, Greve, R., Hoffman, M.J., Humbert, A., Kazmierczak, E., Kleiner, T., Leguy, G.R., Lipscomb, W.H., Martin, D., Morlighem, M., Nowicki, S., Pollard, D., Price, S., Quiquet, A.., Seroussi, H., Schlemm, T., Sutter, J., van de Wal, R.S.W., Winkelmann, R., and Zhang, T.: Antarctic ice sheet response to sudden and sustained ice shelf collapse (ABUMIP). J. Glaciol., in press, 2020.

Thoma, M., Grosfeld, K., Barbi, D., Determann, J., Goeller, S., Mayer, C., and Pattyn, F., RIMBAY – a multi-approximation 3D ice-dynamics model for comprehensive applications: model description and examples. Geosci. Model Dev., 7, 1-21, 2014.

Turcotte, D.L. and Schubert, G.: Geodynamics Applications of Continuum Physics to Geological Problems. J. Wiley Publ., 450 pp, 1982.